Observationally constrained analysis of sulfur cycle in the marine atmosphere with NASA ATom measurements and AeroCom model simulations

Huisheng Bian[1,2], Mian Chin[2], Peter R. Colarco[2], Eric C. Apel[3], Donald R. Blake[4], Karl Froyd[5], Rebecca S. Hornbrook[3], Jose Jimenez[5,6], Pedro Campuzano Jost[5,6], Michael Lawler[5,7], Mingxu Liu[8], Marianne Tronstad Lund[9], Hitoshi Matsui[8], Benjamin A. Nault[5,6,10,11], Joyce E. Penner[12], Andrew W. Rollins[5,13], Gregory Schill[7], Ragnhild B. Skeie[9], Hailong Wang[14], Lu Xu[15,16], Kai Zhang[14], and Jialei Zhu[17]

[1]Goddard Earth Sciences Technology and Research (GESTAR) II, University of Maryland at Baltimore County, Baltimore, MD, USA.
[2]NASA Goddard Space Flight Center, Greenbelt, MD, USA.
[3]Atmospheric Chemistry Observations & Modeling Laboratory, National Center for Atmospheric Research, Boulder, CO, USA.
[4]Department of Chemistry, University of California Irvine, CA, USA.
[5]Cooperative Institute for Research in Environmental Sciences, University of Colorado, Boulder, CO, USA.
[6]Department of Chemistry, University of Colorado, Boulder, CO, USA.
[7]NOAA Chemical Sciences Laboratory, Boulder, CO, USA.
[8]Graduate School of Environmental Studies, Nagoya University, Nagoya, Japan.
[9]CICERO Center for International Climate Research, Oslo, Norway.
[10]Now at: Department of Environmental Health and Engineering, Whiting School of Engineering, The Johns Hopkins, Baltimore, MD, USA.
[11]Now at: Center for Aerosol and Cloud Chemistry, Aerodyne Research, Inc., Billerica, MA, USA
[12]Dept. of Atmospheric, Oceanic and Space Sciences, University of Michigan, Ann Arbor, Michigan, USA.
[13]NOAA Earth System Research Laboratory, Chemical Sciences Division, Boulder, CO, USA.
[14]Atmospheric Sciences and Global Change Division, Pacific Northwest National Laboratory, Richland, WA, USA.
[15]Division of Geological and Planetary Sciences, California Institute of Technology, Pasadena, CA, USA.
[16]Now at Department of Energy, Environmental and Chemical Engineering, Washington University in St. Louis, Missouri, USA.
[17]Institute of Surface-Earth System Science, School of Earth System Science, Tianjin University, Tianjin, China.

Correspondence to: Huisheng Bian (huisheng.bian@nasa.gov)

Abstract

The atmospheric sulfur cycle plays a key role in air quality, climate, and ecosystems, such as pollution, radiative forcing, new particle formation, and acid rain. In this study, we compare the spatially and temporally resolved measurements from the NASA ATom mission with simulations from five AeroCom-III models for four sulfur species (dimethyl sulfide (DMS), sulfur dioxide (SO_2), particulate methanesulfonate (MSA), and particulate sulfate (SO_4)). We focus on remote regions over the Pacific, Atlantic, and Southern Oceans from near the surface to ~12-km altitude range covering all four seasons. In general, the differences among model results can be greater than one-order of magnitude. Comparing with observations, model-simulated SO_2 is generally low wheras SO_4 is generally high. Simulated DMS concentrations near the sea surface exceed observed levels by a factor of five in most cases, suggesting potential overestimation of DMS emissions in all models. With GEOS model simulations of tagging emission from anthropogenic, biomass burning, volcanic, and oceanic sources, we find that anthropogenic emissions are the dominant source of sulfate aerosol (40-60% of the total amount) in the ATom measurements at almost all altitudes, followed by volcanic emissions (18-32%) and oceanic sources (16-32%). Similar source contributions can also be derived at broad ocean basins and on monthly scales, indicating the representativeness of ATom measurements for global ocean. Our work presents the first assessment of AeroCom sulfur study using ATom

Deleted: atmospheric

Deleted: distribution of

Deleted: -containing species,

Deleted: ,

Deleted: that were measured during the airborne NASA Atmospheric Tomography (ATom) mission and simulated by five AeroCom-III models to analyze the budget of sulfur cycle from the models.

Deleted: This study

Deleted: es

Deleted: ocean

Moved down [1]: Our work presents the first assessment of AeroCom sulfur study using ATom measurements, providing directions for improving sulfate simulations, which remain the largest uncertainty in radiative forcing estimates in aerosol climate models.

Deleted: , and

Deleted: s

Deleted: These regions provide us with highly heterogeneous natural and anthropogenic source environments, which is not usually the case for traditional continental studies. We examine the vertical and seasonal variations of these sulfur species over tropical, mid-, and high-latitude regions in both hemispheres. We identify their origins from anthropogenic versus natural sources with sensitivity studies by applying tagged tracers in GEOS model linking to emission types of anthropogenic, biomass burning, volcanic, and oceanic emissions.

Deleted: ile

Deleted: Using interactive oxidant calculation is insufficient to account for model sulfate bias. There are much larger…

Deleted: simulated close to

Deleted: than

Deleted: indicating that the

Formatted: Font color: Red

Formatted: Font color: Red

Deleted: may be too high from

Deleted: The parameterization of converting DMS seawater concentrations into DMS emission fluxes needs to be … [1]

Deleted: A

Deleted: for atmospheric sulfate simulated at location … [2]

Deleted: flight tracks

Deleted: every

Moved (insertion) [1]

Deleted: ,

Deleted: indicating that any reductions of anthropoge … [3]

measurements, providing directions for improving sulfate simulations, which remain the largest uncertainty in radiative forcing estimates in aerosol climate models.

1. Introduction

Atmospheric sulfur species have wide-ranging environmental and health impacts. About two-third of sulfur emissions come from anthropogenic activities (Chin et al., 2000); therefore, considerable efforts have been made to reduce these sulfur emissions. For example, acid rain occurs when sulfur dioxide (SO_2) is oxidized to form sulfuric acid and particulate sulfate (SO_4), which fall to the ground with the rain (Bian et al., 1993; Grennfelt et al., 2020) and can devastate aquatic ecosystems (Josephson et al., 2014; McDonnell et al., 2021). Through the competing neutralization reaction of SO_4 and nitrate with NH_3 and other alkaline species, SO_4 affects strongly both particulate nitrate formation (Bian et al., 2017) and aerosol pH (Huang et al., 2020; Nault et al., 2021). Sulfate is a key component of particulate matter (PM), which degrades air quality (Dong et al., 2018; Tan et al., 2018) and directly reflects the solar radiation (Moch et al., 2022; Myhre et al., 2013). Due to its highly hygroscopic nature, sulfate aerosols act as effcient cloud condensatin nucleus (Boucher et al., 2013; Breen et al., 2021; Seinfeld et al., 2016) and thus indirectly radiative forcing (Penner et al., 2016; Wang et al., 2021) through aerosol-cloud interactions. The contribution of aerosols to atmospheric clouds and energy budget remains the largest uncertainty in climate models (Gryspeerdt et al., 2023; Jia et al., 2021, 2022; Klein et al., 2013; Malavelle et al., 2017). Sulfate is important primarily because the atmospheric sulfate component itself contributes to radiative forcing (RF) almost as much as all other major non-natural aerosol components, as concluded from 16 AeroCom model studies (Myhre et al., 2013). More importantly, uncertainty in sulfate simulations in current climate models is a major contributor to biases in aerosol optical depth (AOD, Fig. 3 in Gliß et al., 2021) and RF (Fig. 7 in Myhre et al., 2013).

Deleted: un's rays

Deleted: affects cloud physics

Deleted: on

Deleted: result

Unlike other major atmospheric aerosols, a significant fraction (i.e., roughly a quarter) of sulfate in the atmosphere comes from marine biological emissions (Chin et al., 1996). The impact of oceanic sulfate is particularly pronounced on marine shallow clouds, which are characterized by low droplet number concentrations and weak updraft velocities (Rissman et al., 2004). Sulfur research has also focused on the tropical upper troposphere (TUT), where the growth of new aerosol particles and homogeneous nucleation involving sulfuric acid is at a maximum (Williamson et al., 2019), and where deep convective transport allows a small portion of the sources to reach the lower stratosphere. The resulting sulfate aerosols in the stratosphere can persist for years (Holton et al., 1995). Unfortunately, the observations in the TUT region and above are sparse. Acquiring atmospheric composition and its chemical/physical properties over remote oceans is challenging, although satellites can often provide total column constraints of aerosol optical depth.

The NASA Earth Venture Suborbital (EVS-2) Atmospheric Tomography (ATom) airborne mission provided abundant measurements of gases and aerosols over the world's oceans (Hodzic et al., 2020; Thompson et al., 2021). In particular, a suite of instruments integrated on the NASA Douglas DC-8 jetliner (hereafter DC-8) made measurements of many important sulfur species including dimethyl sulfide (DMS), SO_2, particulate methanesulfonate (MSA) and SO_4 over the Pacific and Atlantic Oceans in both hemispheres and the Southern Ocean in all four seasons. These regions provide us with highly heterogeneous natural and anthropogenic source

environments, which is not usually the case for traditional continental studies. The comprehensive ATom sulfur dataset provides us with unprecedented opportunities to assess sulfur source, transport, chemistry, deposition, and particle activation and growth represented in the global aerosol models, and to estimate the extent of anthropogenic influence on remote oceanic atmospheric composition and cloud properties.

This study has two specific scientific goals. First, we explore the vertical and seasonal variation of sulfur species (i.e., DMS, SO_2, MSA, and SO_4) using ATom measurements and simulations from five global models that participated in the AeroCom-ATom model experiments. AeroCom is an international initiative of scientists aiming at the advancement of the understanding of the global aerosol and its impact on climate (https://aerocom.met.no/). Here we focus on remote regions over the Pacific, Atlantic, and Southern Oceans, from near the surface to an altitude of about 12 km, covering all four seasons. Second, we determine whether the produced SO_4 originated from anthropogenic or natural sources by using tagged tracers associated with emission types.

Our work is the first study to use ATom measurements for comparison with the AeroCom models, focusing on all sulfur species simulated in current aerosol climate models. This work extends previous efforts using ATom measurements to evaluate the organic carbon (Hodzic et al., 2020) and black carbon (Katich et al., 2018) of AeroCom models, as well as individual models focusing on new particle formation in the tropics (Williamson et al., 2019), fine aerosol lifetime (Gao al. al., 2022), aerosol vertical transport (Yu et al., 2019), sea salt (Bian et al., 2019), smoke (Schill et al., 2020), mineral dust (Froyd et al., 2022), and DMS chemistry (Fung et al., 2022). Furthermore, to our knowledge, there are no studies that systematically investigate the changes and sources of all major sulfur species over the remote ocean. Our study aims not only to reveal sulfur variability based on multiple measurements and model simulations, but also to tease out the underlying processes behind the variability through a comprehensive analysis of simulated sulfur species in aerosol climate models.

The structure of this paper is as follows. Section 2 describes the ATom measurements and the AeroCom models used in this study. Section 3 presents the ATom-AeroCom sulfur comparison from different perspectives, namely the overall comparison in Sect. 3.1, the vertical profiles in Sect. 3.2, and the regional and seasonal analysis in Sect. 3.3. The sulfur budget analysis is given in Sect. 4. We further present investigations of source origins for aerosol SO_4 along flight tracks and over oceans in Sect. 5. Finally, we summarize our findings in Sect. 6.

2. Data

2.1 ATom measurements

ATom was a NASA-funded Earth Venture Suborbital project designed to study the effects of air pollution on chemically reactive gases, aerosols, and greenhouse gases in the remote atmosphere. ATom deployed a large suite of gas and aerosol measurement instruments on the NASA DC-8 aircraft for systematic sampling, covering an extended region of the globe from 85°N to 85°S over the Pacific and Atlantic Oceans, with vertical profiles from near-surface to near-tropopause (i.e., 0.2-12 km, Thompson et al., 2021). Four ATom deployments (ATom-1 to -4) were executed over each of the four seasons from 2016 to 2018, and their flight paths are shown in Fig. 1. The extensive aerosol and gas measurements made during ATom include inorganic and

Deleted: is

Deleted: in

organic aerosols, precursor gases, particle size distributions and particle composition. Table 1 lists the instruments for ATom sulfur species observations used in this study including the relevant sampling details needed for the model comparison.

We use SO_4 and MSA that had been measured by two instruments, the University of Colorado Aerodyne high-resolution time-of-flight aerosol mass spectrometer (AMS, Canagaratna et al., 2007; Guo et al., 2021), and the NOAA Particle Analysis by Laser Mass Spectrometry (PALMS, Froyd et al., 2019). The latter makes *in situ* measurements of the chemical composition of individual aerosol particles. Furthermore, AMS measured submicron aerosols while PALMS provided mass mixing ratio and size distribution up to 3 μm in dry diameter (Brock et al., 2019). It is worth noting that AMS data were independently processed and reported at both 1-s and 60-s time resolutions by instrument PI (Jimenez et al., 2019). The detection limit varied with different averaging time resolutions, and they were provided directly for each sampling point in AMS datasets. Some negative measurements were also presented in AMS datasets, and this is normal for measurements of very low concentrations in the presence of instrumental noise. The AMS data at 60-s resolution is recommended owing to more robust peak fitting at low concentrations (Hodzic et al., 2020). Given the complex data overlays (i.e., starting, ending, and frequency) reported from multiple instruments, the ATom team also provide a 10-s merged dataset to facilitate users' applications. In this study, we evaluate data reported in different time resolutions, using AMS as an example, to ensure the quality of merged data that are exclusively used as the primary dataset in this work.

Two instruments were used for SO_2 measurements: the California Institute of Technology Chemical Ionization Mass Spectrometer (CIMS) and the NOAA Laser Induced Fluorescence (LIF) (Table 1). The CIMS uses CF_3O^- as a reagent ion which reacts with SO_2 via fluoride ion transfer chemistry. The product ion is detected by a compact time-of-flight mass spectrometer (CToF). The precision of the CIMS SO_2 measurement decreases with increasing water vapor concentration (Eger et al., 2019; Huey et al., 2004; Jurkat et al., 2016; Rickly et al., 2021), making it challenging to measure SO_2 in remote ocean regions. In these regions, the ambient water vapor may be sufficiently high that the CIMS SO_2 precision at 1-s resolution (~130 parts per trillion by volume, pptv) is insufficient for measuring ambient SO_2 value there (<100 pptv). To address this shortcoming, the ATom science team added a new instrument, the NOAA LIF, to the ATom-4 payload. The NOAA LIF instrument uses red-shifted laser-induced fluorescence to detect SO_2 at very low ppt levels (Rickly et al., 2021; Rollins et al., 2016). Both instruments report negative values and the detection limit of the LIF instrument is about 2 pptv.

DMS was measured during ATom by two instruments, the University of California, Irvine Whole Air Sampler (WAS), and the NCAR Trace Organic Gas Analyzer (TOGA). The WAS reported DMS for all four ATom deployments, while the TOGA reported data for ATom-2 to -4 and not for ATom-1 due to possible issues associated with the TOGA inlet (the inlet was changed for ATom-2 to -4). Both instruments have comparable detection limit (1 pptv) and accuracy (~15%). However, the sampling time interval of WAS (variable but ~180s) was longer than TOGA (~120s).

2.2 AeroCom models

Five global aerosol models participated in an AeroCom-ATom model experiment (https://wiki.met.no/aerocom/phase3-experiments): CAM-ATRAS, E3SM, GEOS, IMPACT, and OsloCTM3. The experiment required all participating models to (1) conduct three-year-simulations of 2016-2018 (i.e., covering the whole ATom observation period); (2) use or nudge meteorological data for the simulation period; and (3) use the same pre-defined emission fields for precursor gases and aerosol tracers. The suggested emissions are the Coupled Model Intercomparison Project Phase 6 Community Emissions Data System (CEDS, Hoesly et al., 2018) for anthropogenic source, daily biomass burning emission (such as The Global Fire Assimilation System, GFAS), a dataset based on satellite volcanic SO_2 observations from the OMI instrument on the Aura satellite (Carn et al., 2016, 2017) for outgassing and eruptive volcanic emission, and DMS concentration in sea surface from Lana et al. (2011). Wind-driven emissions, such as dust and sea salt, are calculated online by each model. Table 2 summarizes the detailed model characteristics and input datasets relevant to this study. It is worth noting that CEDS specifies anthropogenic emissions from various sectors, including emissions from shipping. The version of CEDS used in this work has emissions up to 2014 and all models use 2014 emission for ATom periods. Furthermore, unlike other models that use CEDS emissions, the anthropogenic emissions of OsloCTM3 are obtained following Shared Socioeconomic Pathways (SSP) under Representative Concentration Pathway (RCP) scenario with medium radiative forcing by the end of the century (SSP245, Fricko et al., 2017), and the emissions are interpolated to 2016 and 2017. Following the experimental protocol, all models provided results for all ATom periods except for OsloCTM3 that omitted data in ATom-4. Unlike traditional AeroCom experiments that used gridded daily/monthly averaged data, modelers are required to interpolate model results along flight track every 10 s (see more discussion in Sect. 3.1) using three-dimensional high frequency (e.g., hourly or even less depending on the models' time step) data to facilitate the comparison. It is worth noting that the models do not have any actual information at 10-s time resolution, given their time steps are at least 10× greater and their spatial resolutions are coarse. However, the interpolation methodology suggested here provides the best model information at their current configuration to compare with aircraft measurements.

The AeroCom-ATom experiment also designed three sensitivity simulations by tracking gas and aerosol emissions to anthropogenic, biomass burning, and volcanic sources to attribute the origin of sulfur sources on sulfur simulations over remote oceans. These experiments were conducted with the Goddard Earth Observing System (GEOS) model. The setup of the GEOS model followed the experiment protocol generally, but GEOS used its own daily biomass burning emissions that were derived from the Quick Fire Emissions Dataset (QFED) developed based on MODIS fire radiative power and calculated in near real-time at 0.1° resolution (Darmenov and da Silva, 2015; Pan et al., 2020). Emissions from biogenic sources were calculated using the Model for Emissions of Gases and Aerosols from Nature (MEGAN) embedded in the GEOS model.

2.3 Tag-tracer study in GEOS

Tag trackers or tags are tied to sources of selected emission types and/or emission locations. Such tag isolates plume from certain activities and is a powerful tool to help understand source attribution or diagnose model performance at the process level. The mechanism behind this technique is that each specific aerosol component in GEOS GOCART is modeled independently of the other components, and the contribution of each emission type to the total aerosol mass is

not disturbed by the other emission types. Therefore, additional aerosol tracers can be easily "tagged" to capture emission type (e.g., anthropogenic, biomass burning, etc.) and location (local, regional or global scale). Tags can be multi-instantiated and computed simultaneously with their baseline counterparts, thereby increasing the computational efficiency of the aerosol models.

Deleted: scientific research.

Tag-tracer technique in GEOS has been widely used in aerosol and gas studies (Bian et al., 2021; Nielsen et al., 2017; Strode et al., 2018) and in supporting various aircraft field campaigns such as Arctic Research of the Composition of the Troposphere from Aircraft and Satellites (ARCTAS) and ATom. Such techniques are also adopted in other models such as GEOS-Chem model (Fisher et al., 2017; Ikeda et al., 2017; Lin et al., 2020) and Community Earth System Model (CESM, Butler et al., 2018).

Four tags linked to emission types of anthropogenic, biomass burning, volcanic, and marine emissions were used in GEOS model to identify anthropogenic versus natural sources of sulfate, and the results are discussed in Sect. 5.

3. ATom-AeroCom comparisons of sulfur species

This section presents a comparison of sulfur species between ATom measurements and AeroCom model simulations. The consistency and diversity of data across remote regimes, both horizontally and vertically, help us understand the effects of emissions, transport, and chemical transformations, and shed light on improving the processes in models to best represent the ATom observations.

3.1 Overall comparison

The overall performance of SO_4 PDF distribution observed from the AMS and PALMS instruments and simulated by five AeroCom models for four ATom deployments is presented in Fig. 2. Also shown in Fig. 2 are the corresponding various percentiles, namely, 0^{th} (minimum), 25^{th}, 50^{th} (median), 75^{th}, and 100^{th} (maximum), and the mean for statistical analyses. The median and mean values are further given in Table S1. The ATom team provided a 10-s merged dataset deliberately by integrating data from various instruments to a unified temporal resolution. We use this 10-s merged data where observations above detection limit (DL) throughout the main text unless otherwise stated. When multiple instruments measured the target field, only points where all instrument measured above DL values were included in analysis, as AMS 10-s in red and PALMS 10-s in grey in Fig. 2. All model results were sampled mimicking flight observations (see Sect. 2.2), and only data with measurements available were used in comparison. This approach ensures that model evaluation is based on high-quality measurements. It is worth noting that the given statistical values in this method represent more regions having high tracer concentration or mixing ratio. In the supplementary material, we further give a model-observation comparison for all available measurement data including negatives.

The mean of PALMS SO_4 is generally about 10-50% higher than AMS SO_4 across four ATom deployments. This performance may be attributed, at least in part, to the fact that the sample size range of PALMS (~3 μm) is larger than that of AMS (~0.75 μm), as mentioned in Sect. 2.1. However, the difference between the two observations is much smaller than the difference

between observation and model. Clearly, the differences in simulated SO_4 among models are high and can easily exceed several orders of magnitude. Most observed and simulated SO_4 exhibit highest probability density around SO_4 values of 10-100 ng sm^{-3}. With the exception of GEOS and CAM-ATRAS, the model SO_4 PDFs show higher tails beyond 100 ng sm^{-3}, which explain the higher median and mean SO_4 simulated by the models. Statistical analysis performed on selected percentiles (box-and-whisker panels in Fig. 2) indicates that multi-model SO_4 medians are about 3.7 (ATom-1), 2.2 (ATom-2), 1.9 (ATom-3), and 1.2 (ATom-4) times higher than observed. In general, nearly all measurements and models indicate that SO_4 concentrations on a global ocean basis are highest during the Northern Hemisphere (NH) spring season (ATom-4). Similar analysis was also performed on all (e.g., both positive and negative) measurement data (Fig. S2), the median/mean values of observations are naturally smaller than those in Fig. 2 by 8-20%, but the PDF distributions are almost identical between the two treatments.

Figure 3 shows the PDF distribution and statistics for SO_2. All observed and simulated data were reprocessed by including points above the detection limit (2 pptv) only. Both instruments (CIMS and LIF) were deployed during ATom-4. Despite CIMS being less precise than LIF (Rollins et al., 2016), both instruments agreed within 95% and CIMS measured SO_2 concentrations were consistently 3-7% lower than LIF measurements. This difference is within the combined uncertainties of the two measurements, but it suggests a systematic calibration difference that is currently unresolved (Rickly et al., 2021). Meanwhile, the width of CIMS SO_2 PDF (measured at half-height) is narrower in ATom-4 than ATom-3, because of improved measurement precision in ATom-4. The CIMS resolution was improved in ATom-4, which enables a better separation of SO_2 and formate-H_2O. The CIMS SO_2 PDF in ATom-4 is around 10 pptv and is more consistent with LIF measurements and model simulations. In contrast, the distribution of SO_2 measured by CIMS during ATom-1 to -3 is spread much wider than the models. Throughout ATom periods, models, especially E3SM, GEOS, and OsloCTM3, show higher peak heights and narrower peak widths. Statistics indicate lower model SO_2 medians than observed (box-and-whisker in Fig. 3), especially during ATom-1. However, the model means are comparable or even higher than those observed, indicating that the models simulate episode events that were not reported in measurements. Consequently, the simulated mean/median ratio is higher than the observed value. Among the four ATom deployments, ATom-4 has much better model observation consistency. Figure S3 presents the corresponding analysis, including the measured negative values. Compared to Fig. 3, the observed median and mean values drop substantially (up to 50%),

Atmospheric DMS observations are scarce, especially on a global scale. Thus, DMS measurements by the two instruments (WAS and TOGA) during the four ATom deployments provide an unprecedented opportunity to investigate biological DMS over global remote oceans and evaluate model DMS simulations on spatial and temporal distributions. By excluding points with measured values below detection limit (i.e., 1 pptv), the overall DMS comparison in Fig. 4 indicates TOGA has higher data peaks and probability densities when DMS ranges from 3-10 pptv. However, this does not appear to be consistent with the lower median and mean values of TOGA, indicating a higher tail in the WAS DMS PDF. Likewise, although the peak of WAS DMS PDF is significantly higher than all models from 3-10 pptv (~5-20 pptv for ATom-3), the median and mean of the WAS DMS are lower, suggesting an even higher tail in model DMS PDF. Overall, there is a big gap between the WAS and TOGA DMS measurements, and both are surprisingly low compared to the models. Statistical analysis performed on selected percentiles

Deleted: unobserved

Deleted: , but the model statistics change relatively small

(the box-and-whisker) indicates that multi-model DMS medians are about 4.9 (ATom-1), 8.6 (ATom-2), 6.6 (ATom-3), and 7.7 (ATom-4) times higher than observed, while model GEOS has a better performance (i.e., 1.2, 2.7, 2.3, and 2.8 correspondingly). The model DMS median values are mostly higher than the observed values. The model DMS mean values are even higher than the observed means (sometimes by more than a factor of 10). This reflects a few very high predicted DMS values. Based on what we know about DMS sources and sinks, these very large simulated DMS appear most commonly in the boundary layer (BL). Indeed it is confirmed in Fig 5 by looking at the ratios of DMS median values between model simulations and observations. The analyses are performed on four vertical ranges (e.g., the entire vertical column, the BL 0-1.5 km, the low-middle free troposphere 1.5-6 km, and the upper troposphere 6-12 km). The last column "MMM/MOM" refers to multi-model median to multi-observation median. The high ratio stems mostly from the BL, above which the consistency is much better. Meanwhile, the PDF distribution and statistics of the models agree better with the WAS measurement than with the TOGA measurement. We should also acknowledge that this is a very limited set of observations we used here, and that there are some longer-term DMS observations near the surface that were used as input for the parameterization of DMS emissions. More DMS observations near the ocean surface are needed to make a confident comparison.

3.2 Vertical profiles

Vertical profiles of ATom-1 to -4 for observed and modeled SO_4, SO_2, DMS, and MSA are shown in Figs. 6-9, respectively, for five latitude bands (from the north to the south) and for both the Pacific and Atlantic Ocean basins. Again, the profiles include equal amounts of data for each measurement and model result. In other words, all comparisons show only available points where the two observed values (i.e., AMS vs. PALMS for SO4 and MSA, CIMS vs. LIF for SO2, and TOGA vs. WAS for DMS) are greater than their detection limits, and where the model values are extracted.

The average and range of sulfur tracers for ATom-1 to -4 are shown in Figs. 6-9 and their corresponding details in each ATom are further given in Figs. S5-8. As shown in Fig. 6, the SO_4 measured by the two instruments are close to each other and lie generally within the range of modelled SO_4 throughout the ATom periods. The spread of modeled SO_4 concentrations is large, exceeding an order of magnitude, especially in the upper troposphere. Despite the need for improvements, the models are generally able to capture the shape of the SO_4 profile. Specifically, CAM-ATRAS and GEOS have good SO_4 vertical gradients over the tropical and NH oceans, but their SO_4 values are too low compared to measurements over the Southern Hemisphere (SH) free troposphere. The SO_4 of IMPACT and OsloCTM3 decreases too slowly with altitude, as shown by their overestimated SO_4 values at high altitudes globally. The results of E3SM are generally within the ranges as predicted by the other models. However, the performance of these models' SO_4 vertical profiles cannot simply be explained by the way the oxidant is applied, because among the five models, CAM-ATRAS, IMPACT, and OsloCTM3 used interactive oxidant calculations, while E3SM and GEOS used archived oxidant data (Table 2). Of the five models, OsloCTM3 and GEOS participated in the multi-model OH assessment (Nicely et al., 2000) and OsloCTM3 had a shorter methane lifetime (relative to OH) than GEOS.

Figure 7 shows generally lower modeled SO_2 volume mixing ratios compared to the CIMS observations for most altitudes and latitude bins. The spread among modeled SO_2 values exceeds

Deleted: Even though the model DMS median is mostly higher than the observed value, the degree of overestimation is not as serious as the mean value that can be more than tenfold, indicating a few points are simulated with extraordinarily high DMS values.

Deleted: span

Deleted: easily

Deleted: E3SM performed SO_4 simulations among other models.…

Deleted: The complexity of the chemistry deserves more attention. …

an order of magnitude around the measured SO_2. SO_2 is better simulated by model IMPACT in the NH than other four AeroCom models and by models CAM-ATRAS and OsloCTM3 in the SH than other three AeroCom models. The tropical Pacific appears to be an interesting region, with all models except GEOS failing to capture observed local SO_2 sources. Basically, the observed SO_2 is high at the surface, falls rapidly in the BL, and then gradually decreases above the BL, except for ATom-1, during which a second peak appears just above the BL (see Fig. S6 for the details of ATom-1 to -4 separately). These observations indicate a strong local source for SO_2 in all seasons and a transport source in the low free-troposphere NH summer (ATom-1). Like observations, the model GEOS predicts a local source for SO_2 at the surface, but it misses the plume above the BL in ATom-1, and its vertical SO_2 convection is consistently too weak. Since only one flight was in ATom-1, more observations are needed to confirm whether GEOS has been failing to catch the plume there during the NH summer. All other models show lower SO_2 at the surface than in the lower free troposphere, which is inconsistent with the observed profiles. Figure S6 also shows an excellent agreement of SO_2 profiles measured by the CIMS and LIF during ATom-4 and models agree with measurements better in ATom-4 as well.

DMS measurements fill in another piece of the puzzle for the atmospheric sulfur budget. As shown in Fig. 8, all five AeroCom models generally overestimate DMS in the BL, particularly for models CAM-ATRAS and OsloCTM3. This large bias close to the surface requires us to revisit the DMS emissions employed in our models. Of the five models, DMS emissions of E3SM, and IMPACT are derived directly from climate emission inventories, while the DMS emission of the other three models are parameterized using monthly climatological DMS concentrations in sea water and surface meteorologies (e.g. surface wind and temperature, see details in Table 3). Specifically, the parameterization used to convert DMS seawater concentrations into DMS emission fluxes was using Nightingale et al. (2000) in CAM-ATRAS and OsloCTM3 and Liss and Merlivat (1986) in GEOS. The three models used two inventories of monthly DMS seawater concentrations, Lana et al. (2011) for CAM-ATRAS and GEOS, and Kettle and Andreae (2000) for OsloCTM3. It is worth noting that even the latest climatological database by Lana et al. (2011) was constructed by compiling measurements before 2000, so the potential long-term change of DMS emission caused by environment change could be missed (Barford, 2013). Also, although the data set used by Lana et al. (2011) is large (i.e., ~47,000 seawater concentration measurements), interpolation and extrapolation techniques were still necessary in creating a global monthly climatological DMS emission. Gali et al. (2018) reported updated oceanic DMS levels on a global scale using remote sensing satellite data. However, much effort is still needed to accurately establish global rates of change in order to create global DMS emissions for climate modeling. This parameterization of air-sea exchange is important because CAM-ATRAS and OsloCTM3, using the same parameterization but different DMS seawater concentrations, reported close emissions in Table 4. On the other hand, the DMS emissions of CAM-ATRAS are almost twice as high as those of GEOS. This difference in emissions results from different parameterizations in the two models, since both models read the same DMS seawater concentration.

Meanwhile, the modeled DMS vertical gradient is generally steeper than the observed one (e.g., Fig. 8 A54N-90N), implying slower vertical transport or faster chemical conversion of DMS to SO_2 in the model. The data submitted by the AeroCom models did not provide us with enough information to obtain the determinants. Currently, GEOS and OsloCTM3 account for two

Deleted: provides

Deleted: Sect.

Deleted: collected from

products from the oxidation of DMS (i.e., SO_2 and MSA) but only GEOS output MSA results. The other models consider DMS oxidation products only as SO_2. These chemical processes in the model may also need to be revisited. Previous studies proposed other chemical reactions for DMS loss in the atmosphere. For example, halogen chemistry represented 71% of the DMS loss in the study of Hoffmann et al. (2016). Veres et al. (2020) estimated that about 30% of DMS in the atmosphere was oxidized to hydroperoxymethyl thioformate (HPMTF), reported only in ATom-4. To this end, the HPMTF serves as a new reservoir of oceanic sulfur and its life cycle in the atmosphere is unknown. The new finding indicates that important components of Earth's sulfur cycle are not yet been fully understood and urges us to reassess this fundamental marine chemical cycle. However, including these chemical DMS losses further reduces DMS above the surface, making DMS in the models even lower at high altitudes.

The GEOS MSA matches observations (Fig. 9) in the lower troposphere. In the upper troposphere (UT), the GEOS MSA tends to decrease slowly or even increase with altitude. These patterns do not agree with observations, and this inconsistency can be explained at least partially by the MSA gas-aerosol partitioning defined in the model and observations. AMS and PALMS only measure the particle phase of MSA, but GEOS MSA is the total MSA and is not accurately represented by observations, especially in UT. Yan et al. (2019) reported that the ratio of MSA to SO_4 can be reduced by 30% when calculations do not consider methanesulfonic acid in the gas phase (MSAg) at low temperatures.

3.3 Regional and seasonal analysis

In order to analyze model performance on a regional and seasonal basis, Figs. 10-12 show histograms of SO_4, SO_2, and DMS concentrations as a function of altitude (rows) and latitudinal band (columns). Only multi-model median is shown here to highlight any common problems in the models. Further details of each individual model are given in Figs. S9-11 and discussed in supplementary material. Each model in this study has its bias at a specific time and location. With the information provided by Figs. S9-11, modelers can further explore the simulation to identify potential causes of model anomalies.

High SO_4 concentration regions vary across seasons (Fig. 10). In the free troposphere (i.e., 1.5 – 12 km), these regions cover the tropics to mid-latitudes in summer and winter (i.e., ATom-1 and ATom-2) and shift to mid- to high-latitudes in spring and autumn (i.e., ATom-3 and ATom-4). The areas with the highest concentration appeared in the SH high-latitudes during ATom-3 (SH spring) and the NH high-latitudes during ATom-4 (NH spring). In the BL, the tropical atmospheric SO_4 concentration appears to be always elevated, and SO_4 concentration levels and SO_4 interregional variation are more pronounced in ATom-1 (NH summer). Among all ATOMs, the performance of the model SO_4 simulation is best for ATom-4 and worst for ATom-1 (NH summer). Compared to observations, model tends to simulate higher SO_4 concentrations in the free troposphere. Both observations and simulations show that the SO_4 over the Pacific is higher than that over the Atlantic during the NH high-latitude autumn (ATom-3) and the NH mid-latitude spring (ATom-4). The differences between observations and simulations are generally larger in the Atlantic than in the Pacific, particularly in the SH. SO_4 concentration levels in simulations and observations can differ significantly in certain areas of each ATom. Differences may be caused by majority models or a few individual models. For example, in summer and winter, the CAM-ATRAS model gave the highest estimates of atmospheric SO_4 in the oceanic

Deleted: a sulfur compound,

Deleted: Of the five models, only GEOS reports MSA (Fig. 9). …

Deleted: phase stages

Deleted: anomalous behavior

Deleted: his knowledge

Deleted: most

Deleted: areas

Deleted: Things are a bit more complicated i

Deleted: but

Deleted: ic atmospher

Deleted: in

Deleted: in

Deleted: ed

Deleted: ed world

BL, but the IMPACT and OsloCTM3 models gave the highest estimates of atmospheric SO_4 in the free troposphere (Fig. S9). All models except the GEOS model generally overestimate SO_4 in the atmosphere.

Atmospheric SO_2 (Fig. 11) is most abundant in the BL of NH mid-latitude Pacific Ocean during ATom-1 (NH summer) and the tropical Pacific BL during ATom-3 (NH autumn), and this high SO_2 region extends to the atmosphere above. Areas where free tropospheric SO_2 concentrations are relatively large do not necessarily follow the example of the BL. For instance, free troposphere appears to be more polluted than other regions in the NH Pacific during ATom-2 and in the SH mid-latitude Atlantic (A40S-20S) during ATom-4, but not in the BL, implying a potential source of SO2 by horizontal transport. The interregional variation of SO_2 in BL is much larger than in the free troposphere, from which local oceanic sources of SO_2 can be inferred. In terms of model-observation comparison, model simulated SO_2 in the free troposphere is generally lower, which is opposite to the case of SO_4. A rapid SO_2 to SO_4 chemical conversion in models could be one of reasons. Fig. S10 further shows individual model SO_2 simulation. For example, the E3SM model gives significantly higher SO_2 compared with the measurements and other models in BL (Fig. S10). Unlike the case of SO_4, all models tend to underestimate SO_2 in the free troposphere, with some exceptions, such as the GEOS model for the mid- to high-latitude North Pacific winter (ATom-2) and the CAM-ATRAS and IMAPCT models for the mid-latitude South Atlantic autumn (ATom-4).

Surface DMS (Fig. 12) is generally higher in the tropics when the ocean is warm and in mid-high latitudes during springtime (e.g., ATom-3 SH spring and ATom-4 NH spring). A remarkable pattern of high model DMS values in the BL is revealed throughout the ATom cycle. This phenomenon also occurs in the free lower troposphere, but not necessarily in the upper troposphere. The high model DMS in BL can be attributed to (1) too high DMS emission, (2) too slow DMS chemical loss, and (3) too slow DMS vertical transport from BL to free troposphere. Additional insight can be obtained by focusing on remote high-latitudes, for example SH high-latitude (40°S-70°S) Pacific, where land source impacts are limited. Thus, the higher simulated SO_2 there in the BL in SYom-4 ruled out a chemical cause due to low DMS loss. The extremely high surface DMS is also not due to the slow vertical transport because simulated DMS is also high in the layers above the BL. A large model DMS emission is likely responsible for the simulated high surface DMS. The overestimation of surface DMS multi-model median in Fig. 12 is clearly attributable to the contribution of all models shown in Fig. S11, with the models CAM-ATRAS and OsloCTM3 being more prominent.

4. Sulfur budget from AeroCom models

Budget analysis is a simple and basic method that has been widely used to document the underlying performance of a model. This analysis allows us to evaluate the AeroCom-III sulfur simulations against previous AeroCom-I and -II studies and serves as a record for future model evaluations. Table 4 summarizes the global sulfur budgets for emissions, wet/dry deposition and chemistry from the five models. Clearly, the largest source of sulfur (~70 TgS/yr) is SO_2 emitted directly from anthropogenic (~78%), biomass burning (~2%), and volcanic sources (~20%). Biogenic DMS (~15-30 TgS) produced and outgassed from decomposition of marine organic molecules provides the largest natural source of sulfur to the atmosphere. A small amount of SO_4 (< 3%) is emitted directly from anthropogenic sources.

Deleted: re

DMS is oxidized in the atmosphere by OH and NO_3 radicals to form SO_2 and MSA. This biological source of SO_2, along with SO_2 emitted directly from other sources, reacts with hydroxyl radicals (OH) in the gas phase and hydrogen peroxide (H_2O_2) and ozone (O_3) in the aqueous phase to produce sulfuric acid (H_2SO_4) and eventually sulfate particles, which play an important role in the formation of clouds over the oceans.

In the five models, DMS predicts the shortest global average lifetime (0.6-2.0 days), followed by SO_2 (1.1-1.8 days), and SO_4 the longest lifetime (3.1-5.6 days). Among them, GEOS has the lowest global burden and shortest lifetime for all sulfur species. The magnitudes of global burdens and lifetimes shown here support the model performance shown in Figs. 2-8. For example, models CAM-ATRAS and OsloCTM3 predicts the highest DMS emission, which is consistent with the highest DMS value (Fig. 4 and S11) and longest lifetime simulated by the two models.

The key budget items include DMS emission, SO_2 emission, sulfate source or total deposition (source and deposition are pretty much the same as expected), lifetime (inversely proportional to the loss rate), and total atmospheric mass load. From the multi-model mean and standard deviation, the diversity can be calculated. Figure 13 shows the global mean budget items in the percentage deviation of each model from the multi-model mean, following the same concept shown in Schulz et al. (2006) and Gliss et al. (2021). It reveals the processes causing model differences. For example, E3SM and GEOS have approximately the same SO_2 emissions and total sulfate sources, but the sulfate lifetime is much shorter in GEOS (implying faster removal rates) thus smaller sulfate burden that is consistent with lower sulfate concentrations in GEOS than in E3SM. At the same time, the lower total sulfate source in E3SM is compensated by longer lifetime compared to CAM-ATRAS, resulting in a comparable global burden of SO_4 in the two models.

It is worth pointing out that the much lower atmospheric SO_4 mass loading of the GEOS simulations is not necessarily related to the poor performance of the GEOS SO_4 simulations, as revealed by the model-measurement comparison in Figs 2, 6 and S9. Although the multi-model mean (or median) often represents the best predictor in the modeling domain, common modeling problems or too small model sample can compromise this effort.

To date, there have been no sulfur budget reports focusing on the vast ocean. However, previous AeroCom studies have reported global sulfate atmospheric loading and its diversity across multiple AeroCom models using monthly and global mean column loadings. Table 5 summarizes these studies, including their reported global and annual sulfate multi-model mean (MMM) and diversity (δ). δ is related to the standard deviation (std_dev) and is defined as δ = std_dev / MMM *100 (%). The results of this work are lower than AeroCom-I but higher than AeroCom-II, which may be related to the different target years involved in these studies. One point to note is that the diversity δ of AeroCom-III models has not reduced since AeroCom-I, which was studied nearly 20 years ago.

5. Source origins for aerosol SO_4 along flight track and Ocean basins

Deleted: has

Deleted: emit

Deleted: re

Deleted: “

Deleted: ”

Deleted: simulation

In this section, we perform an analysis of source attribution by tagging the sulfur source types using the GEOS model. This model is the only one that provides tagged data. Our goal is to understand the sources (anthropogenic, biological, volcanic) of sulfate aerosols in remote regions and how chemistry, transport, and removal processes determine the vertical distribution of sulfate aerosols across seasons and ocean locations.

Figure 14a presents a quantitative summary of the source attribution of aerosol SO_4 sampled along the ATom flight tracks. The analysis was performed over four seasons, spanning the troposphere and three vertical layers (i.e., marine boundary layer, free troposphere and upper troposphere). Overall, anthropogenic emissions were the dominant source (40–60% of the total) of simulated tropospheric SO_4 along the ATom flight tracks for almost all altitudes and seasons, followed by volcanic (18–32%) and oceanic sources (16–32%). Anthropogenic pollution prevailed over remote oceans most in spring and autumn (ATom-3 and -4). The overall contributions from volcanic and oceanic sources are comparable during the ATom periods. Meanwhile, the ocean source contribution has an obvious seasonal variation which is most active during the SH summer (ATom-2), when marine biochemical activity in the vast Southern Ocean is the largest. Volcanos show the largest contribution in the NH summer 2016 (ATom-1) during the four ATom deployments. Given the irregular character of eruptions, the volcanic contribution deserves further discussion below.

In the vertical direction, SO_4 from anthropogenic emissions contributes more than 50% to the free to upper troposphere. Even in the marine boundary layer, anthropogenic sources of SO_4 still account for the largest fraction, except in the SH summer (ATom-2) when oceanic source became dominant. The relative importance of volcanic and marine sources varies not only seasonally but also vertically. Oceanic sources understandably make up a significant fraction (26-42%) of SO_4 in the boundary layer. In the free troposphere, their contribution drops off sharply, reflecting their local surface source characteristics. On the other hand, SO_4 from anthropogenic emissions (including shipping emission) expands in the free troposphere, suggesting that the source originated from distant continental areas. Volcanic SO_4 remains nearly constant throughout the troposphere, making volcanoes the second largest source there. Meanwhile, the contribution of others (OTH including biomass burning) to remote ocean SO_4 is relatively small (< 3%) and will not be discussed further in this study.

The sources of SO_4 discussed above are deduced from the location and timing of the ATom flight path. Conclusions about the total contribution of the ocean needs caution, as there may be representativeness issues using such narrow-band and instantaneous sampling. There might be a situation where, for example, volcanoes provide a very large signal but only account for a small measured area, and in most regions, volcanoes play a very minor role. Whereas oceanic sources in the marine boundary layer perhaps were the dominant source for a much wider region, the SO_4 concentration resulting from the DMS was overall a smaller amount compared to other sources where near a volcanic or anthropogenic source. To address this representation issue, we perform one more analysis with the model data averaged over a wider oceanic region (the shaded area in Fig. 1) and over a longer period (i.e., monthly mean over ATom periods). Such source attributions are given in Fig. 14b.

Deleted: and

Deleted: its

Deleted: its

Deleted: but

Deleted: orchid

Qualitative conclusions drawn from source attribution along the flight tracks generally apply to the ocean basin source attribution, albeit to a slightly different extent. This confirms that continental man-made sources dominate tropospheric SO_4 even over oceans. There is a clear seasonal variation in oceanic contribution, which is largest in austral summer (ATom-2) followed by boreal summer (ATom-1). Concerning volcanic sources, emissions from volcanoes are of two types. One type is the volcanic degassing emissions that tend to remain nearly constant throughout the year and are equivalent to about 20% of SO_2 global anthropogenic emissions. This degassing emission ensures that volcanoes contribute more than 20% to SO_4 over the oceans. The other type consists in the volcanic eruptions. Due to the irregularity of volcanic eruptions in terms of different eruption locations, magnitudes, and times, volcanic eruptions can cause severe fluctuations in SO_4 in the atmosphere. Compared with the source attribution along the flight trajectory, the volcanic contribution decreased over a larger spatial and temporal domain (i.e., ocean basin and monthly mean) in the NH winter 2017 by 32% (ATom-2) and increased in all other three seasons by 14-33%, especially in the NH spring 2018 (ATom-4), when the massive Kilauea eruption in Hawaii began on 3 May 2018. Contrarily, the anthropogenic contribution increased in the NH winter (ATom-2) by 5% and decreased in other seasons by 7-21%.

6. Conclusions

This study investigates sulfur species in remote tropospheric regions at global and seasonal scales using airborne ATom measurements and AeroCom models. The goal is to understand the atmospheric sulfur cycle over the remote oceans, each model's behavior and the spread of model simulations, as well as the observation-model discrepancies. Such understanding and comparison with real observations are crucial to narrow down the uncertainty in model sulfur simulation. Even after decades of development, models are still struggling to accurately simulate sulfur distributions, with differences between models often exceeding an order of magnitude. On the other hand, the agreement between instruments is usually much better. Differences between modeled SO_4 are particularly large in the tropical upper troposphere, where deep convective transport allows a small portion of sulfur to reach the lower stratosphere where sulfate aerosols can persist for many years. Compared with observations, simulated SO_2 is generally low while SO_4 is high. Modeled DMS values are typically an order of magnitude higher than observed DMS near the surface, pointing to a need to revisit the DMS emission inventories and/or the biogeochemical modules used to predict DMS emissions. Our work also suggests investigating three other potential corresponding processes to improve sulfur simulation: whether the chemical conversion from SO_2 to SO_4 is too rapid, whether DMS-generated free tropospheric SO_2 is too low, and whether the vertical transport of DMS and SO_2 from BL to free troposphere is too low. This further investigation requires atmospheric oxidant fields and the ability to track SO_2 production and loss using tagged tracers.

Deleted: sources

Deleted: resultant

We investigate source attribution of SO_4 over remote oceans seasonally and vertically. Sampled at the location and time of ATom measurements, anthropogenic emissions were the dominant source (40–60% of the total) of simulated tropospheric SO_4 at almost all heights and seasons, followed by volcanic (18–32%) and oceanic sources (16–32%). These contributions changed to 34–56%, 17–37%, and 19–37% when extended to the broad Pacific and Atlantic during the months of ATom deployment. This survey confirms that anthropogenic sources dominate tropospheric SO_4 even over oceans. Given that we find DMS source to be overestimated in the

models, the anthropogenic sources overall are a larger portion of the budget, and biogenic is likely smaller than volcanic. Volcanic degassing throughout the year contributes about 20%, and this proportion is increased by explosive eruptions that vary in location and timing. The oceanic contribution has obvious seasonal variation, the largest in the Southern Hemisphere summer, followed by the Northern Hemisphere summer.

It is understood that anthropogenic sulfur emissions currently offset a significant portion of greenhouse gas warming, but they are rapidly declining through emissions controls. As these anthropogenic emissions decrease, natural sources of sulfur, particularly bio-derived sulfur compounds discharged from the world's oceans, will increase their relative contribution. Therefore, more efforts are needed to understand the sulfur cycle in remote environments. On the other hand, our study is the first asserting that anthropogenic emissions remain a major source of sulfate aerosols generated over remote oceans during the ATom deployment periods, suggesting that any limitation of anthropogenic sulfur emissions would have modern global implications.

Even after two decades of development, the diversity of sulfate simulations from AeroCom-I to AeroCom-III has not decreased. However, accurate sulfate simulation in current climate models is crucial to reduce radiative forcing biases. More importantly, apart from the shortcomings of individual models, all modelers involved in this work should focus on the calculation of the air-sea exchange flux formula as it plays a key role in determining DMS emissions. To our knowledge, many other aerosol models employ similar formulas in air-sea flux calculations, so the findings here are applicable to them as well. Modelers also need to study DMS and SO_2 vertical transport as well as SO_4 wet deposition during long-distance transport, as model biases are greatest at high altitudes. One suggestion to modelers is that the use of online oxidant fields is insufficient to explain the model sulfate bias, as there was no systematic bias in the sulfate simulations between the models using interactive oxidants and the models using archival oxidants in this study. The complexity of chemistry deserves more attention.

Deleted: Several potential directions for improving sulfur simulations are suggested above.

Deleted: ,

Code availability. The GEOS Earth System Model source code and the instructions for model build are available at https://github.com/GEOS-ESM/GEOSgcm/ (Last accessed: 28 August 2023).

Data availability. The AeroCom model outputs needed to reproduce the results described in this paper are publicly available for download at https://acd-ext.gsfc.nasa.gov/anonftp/acd/tropo/bian/ATom-AeroCom-Sulfur/. The ATom data was obtained from their ESPO Data Archive: https://espo.nasa.gov/atom/content/ATom, last accessed: 28 August 2022.

Author contributions.
BH and MC conceptualized ATom-AeroCom experiment. BH performed analysis and wrote the manuscript. BH, PRC, MLi, MTL, RBS, HM, JEP, HW, KZ, and JZ provided AeroCom model results and ECA, KF, RSH, JJ, PCJ, MLa, BAN, AWR, GS, and LX contributed to ATom measurements. All authors contributed to the editing of the manuscript.

Competing interests.
At least one of the co-authors is a member of the editorial board of Atmospheric Chemistry and Physics.

Acknowledgements.
HB, MC, and PRC acknowledge the GEOS model developmental efforts at Global Modeling and Assimilation Office (GMAO). This work was supported by NASA's Aura STM and ISFM programs and ACMAP award

(80NSSC23K1000). The computing resources supporting this work were provided by the NASA High-End Computing (HEC) Program through the NASA Center for Climate Simulation (NCCS).
ECA and RSH acknowledge the support of the National Center for Atmospheric Research, which is a major facility sponsored by the National Science Foundation under Cooperative Agreement No. 1852977.
MLi acknowledges the support of JSPS Postdoctoral Fellowships for Research in Japan (Standard).
HM was supported by the Ministry of Education, Culture, Sports, Science, and Technology and the Japan Society for the Promotion of Science (MEXT/JSPS) KAKENHI grants (JP19H05699, JP19KK0265, JP20H00196, JP20H00638, JP22H03722, JP22F22092, JP23H00515, JP23H00523, and JP23K18519); by the MEXT Arctic Challenge for Sustainability II (ArCS II) project (JPMXD1420318865); and by the Environment Research and Technology Development Fund 2-2003 (JPMEERF20202003) and 2-2301 (JPMEERF20232001) of the Environmental Restoration and Conservation Agency.
KZ and HW acknowledge support by the U.S. Department of Energy (DOE), Office of Science, Office of Biological and Environmental Research, Earth and Environmental Systems Modeling program. The Pacific Northwest National Laboratory (PNNL) is operated for DOE by Battelle Memorial Institute under contract DE-AC05-76RLO1830.
LX thanks Michelle Kim, Hannah Allen, John Crounse, and Paul Wennberg for operating the Caltech CIMS instrument during ATom. LX acknowledges NASA grant NNX15AG61A.
MTL thanks Marit Sandstad (CICERO) for assistance with the model post-processing and acknowledges the National Infrastructure for High Performance Computing and Data Storage in Norway (UNINETT) resources (grant NN9188K).
RBS acknowledges funding from the Research Council of Norway (grant number 314997).

References

Abdul-Razzak, H. and Ghan, S.: A parameterization of aerosol acivation, 2. Multiple aerosol types, J. Geophys. Res. Atmos., 105, 6837–6844, https://doi.org/10.1029/1999JD901161, 2000.

Allen, H. M., Bates, K. H., Crounse, J. D., Kim, M. J., Teng, A. P., Ray, E. A., and Wennberg, P. O.: H_2O_2 and CH_3OOH (MHP) in the Remote Atmosphere: 2. Physical and Chemical Controls, J. Geophys. Res. Atmos., 127, e2021JD035702, https://doi.org/10.1029/2021JD035702, 2022.

Bacmeister, J., Suarez, M., and Robertson, F. R.: Rain Reevaporation, Boundary-Layer, Convection Interactions, and Pacific Rainfall Patterns in an AGCM, J. Atmos. Sci., 63, 3383–3403, https://doi.org/10.1175/JAS3791.1, 2006.

Barahona, D. and Nenes, A.: Parameterizing the competition between homogeneous and heterogeneous freezing in cirrus cloud formation – monodisperse ice nuclei, Atmos. Chem. Phys., 9, 369–381, https://doi.org/10.5194/acp-9-369-2009, 2009.

Barahona, D., Molod, A., Bacmeister, J., Nenes, A., Gettelman, A., Morrison, H., Phillips, V., and Eichmann, A.: Development of two-moment cloud microphysics for liquid and ice within the NASA Goddard Earth Observing System Model (GEOS-5), Geosci. Model Dev., 7, 1733–1766, https://doi.org/10.5194/gmd-7-1733-2014, 2014.

Barford, E.: Rising ocean acidity will exacerbate global warming, Nature, https://doi.org/10.1038/nature.2013.13602, 2013.

Bian, H., Luo, C., and Li, X.: Numerical modeling of air pollutant and rainfall effect on acid wet deposition, ACTA Meteorol. Sin., 7, 3, 273–286, 1993.

Bian, H., Chin, M., Hauglustaine, D. A., Schulz, M., Myhre, G., Bauer, S. E., Lund, M. T., Karydis, V. A., Kucsera, T. L., Pan, X., Pozzer, A., Skeie, R. B., Steenrod, S. D., Sudo, K.,

Tsigaridis, K., Tsimpidi, A. P., and Tsyro, S. G.: Investigation of global nitrate from the AeroCom Phase III experiment, Atmos. Chem. Phys., 17, 12911–12940, https://doi.org/10.5194/acp-17-12911-2017, 2017.

Bian, H., Froyd, K., Murphy, D. M., Dibb, J., Darmenov, A., Chin, M., Colarco, P. R., da Silva, A., Kucsera, T. L., Schill, G., Yu, H., Bui, P., Dollner, M., Weinzierl, B., and Smirnov, A.: Observationally constrained analysis of sea salt aerosol in the marine atmosphere, Atmos. Chem. Phys., 19, 10773–10785, https://doi.org/10.5194/acp-19-10773-2019, Aug., 2019.

Bian, H., Lee, E., Koster, R. D., Barahona, D., Chin, M., Colarco, P. R., Darmenov, A., Mahanama, S., Manyin, M., Norris, P., Shilling, J., Yu, H., and Zeng, F.: The response of the Amazon ecosystem to the photosynthetically active radiation fields: integrating impacts of biomass burning aerosol and clouds in the NASA GEOS Earth system model, Atmos. Chem. Phys., 21, 14177–14197, https://doi.org/10.5194/acp-21-14177-2021, 2021.

Boucher, O., Randall, D., Artaxo, P., Bretherton, C., Feingold, G., Forster, P., Kerminen, V.-M., Kondo, Y., Liao, H., Lohmann, U., Rasch, P., Satheesh, S., Sherwood, S., Stevens, B., and Zhang, X.: in: Climate Change 2013: The Physical Science Basis, in: Contribution of Working Group I to the Fifth Assessment Report of the Intergovernmental Panel on Climate Change: Clouds and Aerosols, edited by: Stocker, T., Qin, D., Plattner, G.-K., Tignor, M., Allen, S., Boschung, J., Nauels, A., Xia, Y., Bex, V., and Midgley, P., Cambridge University Press, Cambridge, UK and New York, NY, USA, 571–657, 2013.

Breen, K. H., Barahona, D., Yuan, T., Bian, H., and James, S. C., Effect of volcanic emissions on clouds during the 2008 and 2018, Atmos. Chem. Phys., 21, 7749–7771, https://doi.org/10.5194/acp-21-7749-2021, 2021.

Brock, C. A., Williamson, C., Kupc, A., Froyd, K. D., Erdesz, F., Wagner, N., Richardson, M., Schwarz, J. P., Gao, R.-S., Katich, J. M., Campuzano-Jost, P., Nault, B. A., Schroder, J. C., Jimenez, J. L., Weinzierl, B., Dollner, M., Bui, T., and Murphy, D. M.: Aerosol size distributions during the Atmospheric Tomography Mission (ATom): methods, uncertainties, and data products, Atmos. Meas. Tech., 12, 3081–3099, 2019.

Butler, T., Lupascu, A., Coates, J., and Zhu, S.: TOAST 1.0: Tropospheric Ozone Attribution of Sources with Tagging for CESM 1.2.2, Geosci. Model Dev., 11, 2825–2840, https://doi.org/10.5194/gmd-11-2825-2018, 2018.

Carn, S. A., Clarisse, L., and Prata, A. J.: Multi-decadal satellite measurements of global volcanic degassing, J. Volcanol. Geotherm. Res., 311, 99–134, http://dx.doi.org/10.1016/j.jvolgeores.2016.01.002, 2016.

Carn, S. A., Fioletov, V. E., McLinden, C. A., and Krotkov, N. A.: A decade of global volcanic SO_2 emissions measured from space, Sci. Rep., 7, 44095, https://doi.org/10.1038/srep44095, 2017.

Chin, M., Rood, R. B., Lin, S. J., Müller, J.-F., and Thompson, A. M.: Atmospheric sulfur cycle simulated in the global model GOCART: model description and global properties, J. Geophys. Res. Atmos., 105, D20, 24671–24687, https://doi.org/10.1029/2000JD900384, 2000.

Colarco, P. R., da Silva, A., Chin, M., and Diehl, T.: Online simulations of global aerosol distributions in the NASA GEOS-4 model and comparisons to satellite and ground-based aerosol optical depth, J. Geophys. Res. Atmos., 115, D14207, https://doi.org/10.1029/2009JD012820, 2010.

Crounse, J. D., McKinney, K. A., Kwan, A., J. and Wennberg, P. O., Measurement of Gas-Phase Hydroperoxides by Chemical Ionization Mass Spectrometry, Anal. Chem., 78, 19, 6726–6732, https://doi.org/10.1021/ac0604235, 2006.

Darmenov, A. and da Silva, A.: The Quick Fire Emissions Dataset (QFED) - Documentation of versions 2.1, 2.2 and 2.4, NASA TM-2015-104606, Vol. 38, 183 pp., 2015.

Dentener, F., et al. (2006). "Emissions of primary aerosol and precursor gases in the years 2000 and 1750 prescribed data-sets for AeroCom." Atmospheric Chemistry and Physics 6: 4321-4344.

Dong, X., Fu, J. S., Zhu, Q., Sun, J., Tan, J., Keating, T., Sekiya, T., Sudo, K., Emmons, L., Tilmes, S., Jonson, J. E., Schulz, M., Bian, H., Chin, M., Davila, Y., Henze, D., Takemura, T., Benedictow, A. M. K., and Huang, K.: Long-range transport impacts on surface aerosol concentrations and the contributions to haze events in China: an HTAP2 multi-model study, Atmos. Chem. Phys., 18, 15581-15600, https://doi.org/10.5194/acp-18-15581-2018, 2018.

Eger, P. G., Helleis, F., Schuster, G., Phillips, G. J., Lelieveld, J., and Crowley, J. N.: Chemical ionization quadrupole mass spectrometer with an electrical discharge ion source for atmospheric trace gas measurement, Atmos. Meas. Tech., 12, 1935–1954, https://doi.org/10.5194/amt-12-1935-2019, 2019.

Feng, L., Smith, S. J., Braun, C., Crippa, M., Gidden, M. J., Hoesly, R., Klimont, Z., van Marle, M., van den Berg, M., and van der Werf, G. R.: The generation of gridded emissions data for CMIP6, Geosci. Model Dev., 13, 461–482, https://doi.org/10.5194/gmd-13-461-2020, 2020.

Fisher, J. A., Murray, L. T., Jones, D. B. A., and Deutscher, N. M.: Improved method for linear carbon monoxide simulation and source attribution in atmospheric chemistry models illustrated using GEOS-Chem v9, Geosci. Model Dev., 10, 4129–4144, https://doi.org/10.5194/gmd-10-4129-2017, 2017.

Fountoukis, C. and Nenes, A.: Continued development of a cloud droplet formation parameterization for global climate models, J. Geophys. Res. Atmos., 110, D11212, https://doi.org/10.1029/2004JD005591, 2005.

Fricko O., Havlik P., Rogelj J., Klimont Z., Gusti M., Johnson N., Kolp P., Strubegger M., Valin H., Amann M., Ermolieva, T., Forsell, N., Herrero, M. , Heyes, C., Kindermann, G., Volker Krey, V., McCollum, D. L., Obersteiner, M., Shonali Pachauri, S., Shilpa Rao, S., Riahi,

K., The marker quantification of the Shared Socioeconomic Pathway 2: a middle-of-the-road scenario for the 21st century. Glob. Environ. Change, 42, 251–267, 2017.

Froyd, K. D., Yu, P., Schill, G. P., Brock, C. A., Kupc, A., Williamson, C. J., Jensen, E. J. Ray, E., Rosenlof, K. H., Bian, H., Darmenov, A. S., Colarco, P. R., Diskin, G. S., Bui, T. P., and Murphy, D. M., Global-scale measurements reveal cirrus clouds are seeded by mineral dust aerosol, Nat. Geosci., Volume 15, Issue 3, p.177-183, 10.1038/s41561-022-00901-w, Feb, 2022.

Fung K. M., Heald, C.L., Kroll, J.H., Wang, S., Jo, D.S., Gettelman, A., Lu, Z., Liu, X., Zaveri, R. A., Apel, E. C., Blake, D., R., Jimenez, J., Campuzano-Jost, P., Veres, P. R., Bates, T. S.,Shilling, J. E., and Zawadowicz. M., Exploring dimethyl sulfide (DMS) oxidation and implications for global aerosol radiative forcing. Atmos. Chem. and Phys., 22, 2:1549-1573, PNNL-SA-166358, https://doi:10.5194/acp-22-1549-2022, 2022.

Galí, M., Levasseur, M., Devred, E., Simó, R., and Babin, M.: Sea-surface dimethylsulfide (DMS) concentration from satellite data at global and regional scales, Biogeosciences, 15, 3497–3519, https://doi.org/10.5194/bg-15-3497-2018, 2018.

Gao, C. Y., Heald, C. L., Katich, J. M., Luo, G., Yu, F., Remote Aerosol Simulated During the Atmospheric Tomography (ATom) Campaign and Implications for Aerosol Lifetime, J. Geophys. Res. Atoms., Vol. 127, I. 22, https://doi.org/10.1029/2022JD036524, 2022.

Gliß, J., Mortier, A., Schulz, M., Andrews, E., Balkanski, Y., Bauer, S. E., Benedictow, A. M. K., Bian, H., Checa-Garcia, R., Chin, M., Ginoux, P., Griesfeller, J. J., Heckel, A., Kipling, Z., Kirkevåg, A., Kokkola, H., Laj, P., Le Sager, P., Lund, M. T., Lund Myhre, C., Matsui, H., Myhre, G., Neubauer, D., van Noije, T., North, P., Olivié, D. J. L., Rémy, S., Sogacheva, L., Takemura, T., Tsigaridis, K., and Tsyro, S. G.: AeroCom phase III multi-model evaluation of the aerosol life cycle and optical properties using ground- and space-based remote sensing as well as surface in situ observations, Atmos. Chem. Phys., 21, 87–128, https://doi.org/10.5194/acp-21-87-2021, Jan., 2021.

Grennfelt, P., Engleryd, A., Forsius, M., Hov, Ø., Rodhe, H., and Cowling, E.: Acid rain and air pollution: 50 years of progress in environmental science and policy, Ambio, 49, 849–864, https://doi.org/10.1007/s13280-019-01244-4, 2020.

Gryspeerdt, E., Povey, A. C., Grainger, R. G., Hasekamp, O., Hsu, N. C., Mulcahy, J. P., Sayer, A. M., and Sorooshian, A.: Uncertainty in aerosol-cloud radiative forcing is driven by clean conditions, Atmos. Chem. Phys., 23, 4115–4122, https://doi.org/10.5194/acp-23-4115-2023, 2023.

Guo, H., Campuzano-Jost, P., Nault, B. A., Day, D. A., Schroder, J. C., Kim, D., Dibb, J. E., Dollner, M., Weinzierl, B., and Jimenez, J. L.: The importance of size ranges in aerosol instrument intercomparisons: a case study for the Atmospheric Tomography Mission, Atmos. Meas. Tech., 14, 3631–3655, 2021.

Hodshire, A. L., Campuzano-Jost, P., Kodros, J. K., Croft, B., Nault, B. A., Schroder, J. C., Jimenez, J. L., and Pierce, J. R.: The potential role of methanesulfonic acid (MSA) in aerosol formation and growth and the associated radiative forcings, Atmos. Chem. Phys., 19, 3137–3160, 2019.

Hodzic, A., Campuzano-Jost, P., Bian, H., Chin, M., Colarco, P. R., Day, D. A., Froyd, K. D., Heinold, B., Jo, D. S., Katich, J. M., Kodros, J. K., Nault, B. A., Pierce, J. R., Ray, E., Schacht, J., Schill, G. P., Schroder, J. C., Schwarz, J. P., Sueper, D. T., Tegen, I., Tilmes, S., Tsigaridis, K., Yu, P., and Jimenez, J. L.: Characterization of organic aerosol across the global remote troposphere: a comparison of ATom measurements and global chemistry models, Atmos. Chem. Phys., 20, 4607–4635, 2020.

Hoffmann, E. H., Tilgner, A., Schrödner, R., Bräuer, P., Wolke, R. and Herrmann, H., An advanced modeling study on the impacts and atmospheric implications of multiphase dimethyl sulfide chemistry, Proc. Natl. Acad. Sci. USA, 113, 11776–11781, https://doi.org/10.1073/pnas.1606320113, 2016.

Holton, J. R., Haynes, P. H., McIntyre, M. E., Douglass, A. R., Rood, R. B., and Pfister, L.: Stratosphere-troposphere exchange, Rev. Geophys., 33, 403–439, https://doi.org/10.1029/95RG02097, 1995.

Hoesly, R. M., Smith, S. J., Feng, L., Klimont, Z., Janssens-Maenhout, G., Pitkanen, T., et al. (2018). Historical (1750–2014) anthropogenic emissions of reactive gases and aerosols from the Community Emissions Data System (CEDS). Geosci. Model Dev., 11, 369–408. https://doi.org/10.5194/gmd-11-369-2018.

Huang, R-J., Duan, J., Li, Y., Chen, Q., Chen, Y., Tang, M., Yang, L., Ni, H., Lin, C., Xu, W., Liu, Y., Chen, C., Yan, Z., Ovadnevaite, J., Ceburnis, D., Dusek, U., Cao, J., Hoffmann, T., & O'Dowd, C. D., Effects of NH3 and alkaline metals on the formation of particulate sulfate and nitrate in wintertime Beijing. Sci. Total Environ., 717, 137190, https://doi.org/10.1016/j.scitotenv.2020.137190, 2020.

Huey, L. G., Tanner, D. J., Slusher, D. L., Dibb, J. E., Arimoto, R., Chen, G., Davis, D., Buhr, M. P., Nowak, J. B., Mauldin III, R. L., Eisele, F. L., and Kosciuch, E.: CIMS measurements of HNO_3 and SO_2 at the South Pole during ISCAT 2000, Atmos. Environ., 38, 5411–5421, https://doi.org/10.1016/j.atmosenv.2004.04.037, 2004.

Ikeda, K., Tanimoto, H., Sugita, T., Akiyoshi, H., Kanaya, Y., Zhu, C., and Taketani, F.: Tagged tracer simulations of black carbon in the Arctic: transport, source contributions, and budget, Atmos. Chem. Phys., 17, 10515–10533, https://doi.org/10.5194/acp-17-10515-2017, 2017.

Jia, H., Ma, X., Yu, F., and Quaas, J.: Significant underestimation of radiative forcing by aerosol–cloud interactions derived from satellite-based methods, Nat. Commun., 12, https://doi.org/10.1038/s41467-021-23888-1, 2021.

Jia, H., Quaas, J., Gryspeerdt, E., Böhm, C., and Sourdeval, O.: Addressing the difficulties in quantifying the Twomey effect for marine warm clouds from multi-sensor satellite observations

and reanalysis, Atmos. Chem. Phys., 22, 7353–7372, https://doi.org/10.5194/acp-22-7353-2022, 2022.

Lin, X., Keppel-Aleks, G., Rogers, B. M., Birch, L.: Simulated CO2 tracer concentrations in the Northern Hemisphere from a tagged transport model GEOS-Chem v12.0.0 [Data set], University of Michigan - Deep Blue Data. https://doi.org/10.7302/rp59-rw53, 2020.

Moch, J. M., Mickley, L. J., Keller, C. A., Bian, H., Lundgren, E. W., Zhai, S., and Jacob, D. J.: Aerosol-radiation interactions in China in winter: Competing effects of reduced shortwave radiation and cloud-snowfall-albedo feedbacks under rapidly changing emissions, J. Geophys. Res. Atmos., 127, e2021JD035442, https://doi.org/10.1029/2021JD035442, 2022.

Myhre, G., B. H., Samset, M. Schulz, Y. Balkanski, S. Bauer, T. K. Berntsen, H. Bian, N. Bellouin, M. Chin, T. Diehl, R. C. Easter, J. Feichter, S. J. Ghan, D. Hauglustaine, T. Iversen, S. Kinne, A. Kirkevåg, J.-F. Lamarque, G. Lin, X. Liu, G. Luo, X. Ma, J. E. Penner, P. J. Rasch, Ø. Seland, R. B. Skeie, P. Stier, T. Takemura, K. Tsigaridis, Z. Wang, L. Xu, H. Yu, F. Yu, J.-H. Yoon, K. Zhang, H. Zhang, and C. Zhou, Radiative forcing of the direct aerosol effect from AeroCom Phase II simulations, Atmos. Chem. Phys., 13, 1853-1877, doi:10.5194/acp-13-1853-2013, 2013.

Josephson, D. C., Robinson, J. M., Chiotti, J,, Jirka, K. J., and Kraft, C. E.: Chemical and biological recovery from acid deposition within the Honnedaga Lake watershed, New York, USA, Environ. Monit. Assess., 186, 4391–4409, https://doi.org/10.1007/s10661-014-3706-9, 2014.

Jurkat, T., Kaufmann, S., Voigt, C., Schäuble, D., Jeßberger, P., and Ziereis, H.: The airborne mass spectrometer AIMS – Part 2: Measurements of trace gases with stratospheric or tropo-spheric origin in the UTLS, Atmos. Meas. Tech., 9, 1907–1923, https://doi.org/10.5194/amt-9-1907-2016, 2016.

Katich, J. M., Samset, B. H., Paul Bui, T., Dollner, M., Froyd, K. D., Campuzano-Jost, P., Nault, B. A., Schroder, J. C., Weinzierl, B., Schwarz J. P., Strong Contrast in Remote Black Carbon Aerosol Loadings Between the Atlantic and Pacific Basins, Journal of Geophysical Research: Atmospheres, Volume 123, Issue 23 p. 13,386-13,395, https://doi.org/10.1029/2018JD029206, 2018.

Kettle, A. J. and Andreae, M. O.: Flux of dimethylsulfide from the oceans: A comparison of updated data sets and flux models, J. Geophys. Res. Atmos., 105, 26793–26808, https://doi.org/10.1029/2000JD900252, 2000.

Klein, S. A., Zhang, Y., Zelinka, M. D., Pincus, R., Boyle, J., and Gleckler, P. J.: Are climate model simulations of clouds improving? An evaluation using the ISCCP simulator, J. Geophys. Res. Atmos., 118, 1329–1342, https://doi.org/10.1002/jgrd.50141, 2013.

Lana, A., Bell, T. G., Simó, R., Vallina, S. M., Ballabrera-Poy, J., Kettle, A. J., Dachs, J., Bopp, L., Saltzman, E. S., Stefels, J., Johnson, J. E., and Liss, P. S.: An updated climatology of surface

dimethlysulfide concentrations and emission fluxes in the global ocean, Global Biogeochem. Cy., 25, GB1004, doi:10.1029/2010GB003850, 2011.

Liss, P.S., and Merlivat, L., Air-sea gas exchange rates: Introduction and synthesis, in The Role of Air-Sea Gas Exchange in Geochemical Cycling, edited by P. Buat-Menard, pp. 113-127, D. Reidel, Norwell, Mass., 1986.

Liu, M. and Matsui, H.: Improved simulations of global black carbon distributions by modifying wet scavenging processes in convective and mixed-phase clouds, J. Geophys. Res. Atmos., 126, e2020JD033890, https://doi.org/10.1029/2020JD033890, 2021.

Lund, M. T., Myhre, G., Haslerud, A. S., Skeie, R. B., Griesfeller, J., Platt, S. M., Kumar, R., Myhre, C. L., and Schulz, M.: Concentrations and radiative forcing of anthropogenic aerosols from 1750 to 2014 simulated with the Oslo CTM3 and CEDS emission inventory, Geosci. Model Dev., 11, 4909–4931, https://doi.org/10.5194/gmd-11-4909-2018, 2018.

Malavelle, F. F., Haywood, J. M., Jones, A., Gettelman, A., Clarisse, L., Bauduin, S., Allan, R. P., Karset, I. H. H., Kristjánsson, J. E., Oreopoulos, L., Cho, N., Lee, D., Bellouin, N., Boucher, O., Grosvenor, D. P., Carslaw, K. S., Dhomse, S., Mann, G. W., Schmidt, A., Coe, H., Hartley, M. E., Dalvi, M., Hill, A. A., Johnson, B. T., Johnson, C. E., Knight, J. R., O'Connor, F. M., Partridge, D. G., Stier, P., Myhre, G., Platnick, S., Stephens, G. L., Takahashi, H., and Thordarson, T.: Strong constraints on aerosol–cloud interactions from volcanic eruptions, Nature, 546, 485-491, https://doi.org/10.1038/nature22974, 2017.

McDonnell, T. C., Driscoll, C. T., Sullivan, T. J., Burns, D. A., Baldigo, B. P., Shao, S., and Lawrence, G. B.: Regional target loads of atmospheric nitrogen and sulfur deposition for the protection of stream and watershed soil resources of the Adirondack Mountains, USA, Environ. Pollut., 281, 117110, https://doi.org/10.1016/j.envpol.2021.117110, 2021.

Matsui, H.: Development of a global aerosol model using a two-dimensional sectional method: 1. Model design, J. Adv. Model. Earth Syst., 9, 1921–1947, https://doi.org/10.1002/2017MS000936, 2017.

Matsui, H. and Mahowald, N.: Development of a global aerosol model using a two-dimensional sectional method: 2. Evaluation and sensitivity simulations, J. Adv. Model. Earth Syst., 9, 1887–1920, https://doi.org/10.1002/2017MS000937, 2017.

Molod, A.: Constraints on the Total Water PDF in GCMs from AIRS and a High Resolution Model, J. Climate, 25, 8341–8352, https://doi.org/10.1175/JCLI-D-11-00412.1, 2012.

Moorthi, S. and Suarez, M. J.: Relaxed Arakawa-Schubert. A parameterization of moist convection for general circulation models, Mon. Weather Rev., 120, 978–1002, https://doi.org/10.1175/1520-0493(1992)120<0978:RASAPO>2.0.CO;2, 1992.

Myhre, G., Samset, B. H., Schulz, M., Balkanski, Y., Bauer, S., Berntsen, T. K., Bian, H., Bellouin, N., Chin, M., Diehl, T., Easter, R. C., Feichter, J., Ghan, S. J., Hauglustaine, D.,

Iversen, T., Kinne, S., Kirkevåg, A., Lamarque, J.-F., Lin, G., Liu, X., Lund, M. T., Luo, G., Ma, X., van Noije, T., Penner, J. E., Rasch, P. J., Ruiz, A., Seland, Ø., Skeie, R. B., Stier, P., Takemura, T., Tsigaridis, K., Wang, P., Wang, Z., Xu, L., Yu, H., Yu, F., Yoon, J.-H., Zhang, K., Zhang, H., and Zhou, C.: Radiative forcing of the direct aerosol effect from AeroCom Phase II simulations, Atmos. Chem. Phys., 13, 1853–1877, https://doi.org/10.5194/acp-13-1853-2013, 2013.

Nicely, J. M., Duncan, B. N., Hanisco, T. F., Wolfe, G. M., Salawitch, R. J., Deushi, M., Haslerud, A. S., Jöckel, P., Josse, B., Kinnison, D. E., Klekociuk, A., Manyin, M. E., Marécal, V., Morgenstern, O., Murray, L. T., Myhre, G., Oman, L. D., Pitari, G., Pozzer, A., Quaglia, I., Revell, L. E., Rozanov, E., Stenke, A., Stone, K., Strahan, S., Tilmes, S., Tost, H., Westervelt, D. M., and Zeng, G.: A machine learning examination of hydroxyl radical differences among model simulations for CCMI-1, Atmos. Chem. Phys., 20, 1341–1361, https://doi.org/10.5194/acp-20-1341-2020, 2020.

Nielsen, J. E., Pawson, S., Molod, A., Auer, B., da Silva, A. M., Douglass, A. R., Wargan, K.: Chemical mechanisms and their applications in the Goddard Earth Observing System (GEOS) earth system model. J. Adv. Model. Earth Sys., 9, 3019–3044. https://doi.org/10.1002/2017MS001011, 2017.

Nightingale P. D., Malin G., Law C. S., Watson A. J., Liss P. S., Liddicoat M. I., et al. In situ evaluation of air-sea gas exchange parameterizations using novel conservative and volatile tracers. Global Biogeochem. Cy. 14, 373–387, https://doi.org/10.1029/1999gb900091, 2000.

Penner, A., Prather, J. E., Ramanathan, K. A., Ramaswamy, V., Rasch, V., Ravishankara, P. J., Rosenfeld, A. R., Stephens, D., and Wood, R.: Improving our fundamental understanding of the role of aerosol–cloud interactions in the climate system, P. Natl. Acad. Sci. USA, 113, 5781–5790, https://doi.org/10.1073/pnas.1514043113, 2016.

Rasch, P. J., Xie, S., Ma, P. -L., Lin, W., Wang, H., Tang, Q., Burrows, S. M., Caldwell, P., Zhang, K., Easter, R. C., Cameron-Smith, P., Singh, B., Wan, H., Golaz, J.-C., Harrop, B. E., Roesler, E., Bacmeister, J., Larson, V. E., Evans, K. J., Qian, Y., Taylor, M., Leung, L. R., Zhang, Y., Brent, L., Branstetter, M., Hannay, C., Mahajan, S., Mametjanov, A., Neale, R., Richter, J. H., Yoon, J.-H., Zender, C. S., Bader, D., Flanner, M., Foucar, J. G., Jacob, R., Keen, N., Klein, S. A., Liu, X., Salinger, A. G., Shrivastava, M., and Yang, Y.: An Overview of the Atmospheric Component of the Energy Exascale Earth System Model, J. Adv. Model. Earth Syst., 11, 2377–2411, https://doi.org/10.1029/2019MS001629, 2019.

Rickly, P. S., Xu, L., Crounse, J. D., Wennberg, P. O., and Rollins, A. W.: Improvements to a laser-induced fluorescence instrument for measuring SO_2 – impact on accuracy and precision, Atmos. Meas. Tech., 14, 2429–2439, https://doi.org/10.5194/amt-14-2429-2021, 2021.

Rienecker, M., Suarez, M., Todling, R., Bacmeister, J., Takacs, L., Liu, H.-C., Gu, W., Sienkiewicz, M., Koster, R., Gelaro, R., Stajner, I., and Nielsen, J.: The GEOS-5 Data Assimilation System – Documentation of Versions 5.0.1, 5.1.0, and 5.2.0., Vol. 27 of Technical

Report Series on Global Modeling and Data Assimilation, NASA Goddard Space Flight Center, Greenbelt, MD, USA, 2008.

Rissman, T. A., Nenes, A., and Seinfeld, J. H.: Chemical amplification (or dampening) of the Twomey effect: Conditions derived from droplet activation theory, J. Atmos. Sci., 61(8), 919–930, https://doi.org/10.1175/1520-0469(2004)061<0919:CAODOT>2.0.CO;2, 2004.

Rollins, A. W., Thornberry, T. D., Ciciora, S. J., McLaughlin, R. J., Watts, L. A., Hanisco, T. F., Baumann, E., Giorgetta, F. R., Bui, T. V., Fahey, D. W., and Gao, R.-S.: A laser-induced fluorescence instrument for aircraft measurements of sulfur dioxide in the upper troposphere and lower stratosphere, Atmos. Meas. Tech., 9, 4601–4613, https://doi.org/10.5194/amt-9-4601-2016, 2016.

Saltzman, E. S., King, D. B., Holmen, K., and Leck, C., Experimental Determination of the Diffusion Coefficient of Dimethylsulfide in Water, J. of Geophys. Res. Atoms., Vol. 98, No. C9, 16,481-16,486, 1993.

Schill, G. P., Froyd, K. D., Bian, H., Kupc, A., Williamson, C., Brock, C. B., Ray, E., Hornbrook, R. S., Hills, A. J., Apel, E. C., Chen, M., Colarco, P., and Murphy, D. M., The ubiquity of dilute, aged smoke in the global remote troposphere and its effect on climate, Nature Geoscience, 13(6), https://doi:10.1038/s41561-020-0586-1, Jun., 2020.

Schueneman, M. K., Nault, B. A., Campuzano-Jost, P., Jo, D. S., Day, D. A., Schroder, J. C., Palm, B. B., Hodzic, A., Dibb, J. E., and Jimenez, J. L.: Aerosol pH indicator and organosulfate detectability from aerosol mass spectrometry measurements, Atmos. Meas. Tech., 14, 2237–2260, 2021.

Seinfeld, J. H., Bretherton, C., Carslaw, K. S., Coe, H., DeMott, P. J., Dunlea, E. J., Feingold, G., Ghan, S., Guenther, A. B., Kahn, R., Kraucunas, I., Kreidenweis, S. M., Molina, M. J., Nenes, A., Penner, J. E., Prather, K. A., Ramanathan, V., Ramaswamy, V., Rasch, P. J., Ravishankara, A. R., Rosenfeld, D., Stephens, G., and Wood, R.: Improving our fundamental understanding of the role of aerosol–cloud interactions in the climate system, P. Natl. Acad. Sci. USA, 113, 5781–5790, https://doi.org/10.1073/pnas.151404311, 2016.

Schulz, M., Textor, C., Kinne, S., Balkanski, Y., Bauer, S., Berntsen, T., Berglen, T., Boucher, O., Dentener, F., Guibert, S., Isaksen, I. S. A., Iversen, T., Koch, D., Kirkevåg, A., Liu, X., Montanaro, V., Myhre, G., Penner, J. E., Pitari, G., Reddy, S., Seland, Ø., Stier, P., and Takemura, T.: Radiative forcing by aerosols as derived from the AeroCom present-day and pre-industrial simulations, Atmos. Chem. Phys., 6, 5225–5246, https://doi.org/10.5194/acp-6-5225-2006, 2006

Simpson, I. J., Colman, J. J., Swanson, A. L., Bandy, A. R., Thornton, D. C., Blake, D. R., and F. S. Rowland, F. S.: Aircraft Measurements of Dimethyl Sulfide (DMS) Using a Whole Air Sampling Technique, J. Atmos. Chem., 39, 191-213, https://doi.org/10.1023/A:1010608529779, 2001.

Slingo, J.: The development and verification of a cloud prediction scheme for the ECMWF model, Q. J. Roy. Meteor. Soc., 113, 899–927, https://doi.org/10.1002/qj.49711347710, 1987.

Smith, R. N. B.: A scheme for predicting layer clouds and their water content in a general circulation model, Q. J. Roy. Meteor. Soc., 116, 435–460, https://doi.org/10.1002/qj.49711649210, 1990.

Søvde, O. A., Prather, M. J., Isaksen, I. S. A., Berntsen, T. K., Stordal, F., Zhu, X., Holmes, C. D., and Hsu, J.: The chemical transport model Oslo CTM3, Geosci. Model Dev., 5, 1441–1469, https://doi.org/10.5194/gmd-5-1441-2012, 2012.

Strode, S. A., Liu, J., Lait, L., Commane, R., Daube, B., Wofsy, S., Conaty, A., Newman, P., and Prather, M.: Forecasting carbon monoxide on a global scale for the ATom-1 aircraft mission: insights from airborne and satellite observations and modeling, Atmos. Chem. Phys., 18, 10955–10971, https://doi.org/10.5194/acp-18-10955-2018, 2018.

Tan, J., Fu, J. S., Dentener, F., Sun, J., Emmons, L., Tilmes, S., Flemming, J., Takemura, T., Bian, H., Zhu, Q., Yang, C.-E., and Keating, T.: Source contributions to sulfur and nitrogen deposition – an HTAP II multi-model study on hemispheric transport, Atmos. Chem. Phys., 18, 12223–12240, https://doi.org/10.5194/acp-18-12223-2018, 2018.

Thompson, C. R., Wofsy, S. C., Prather, M. J., Newman, P. A., Hanisco, T. F., Ryerson, T. B., Fahey, D. W., Apel, E. C., Brock, C. A., Brune, W. H., Froyd, K., Katich, J. M., Nicely, J. M., Peischl, J., Ray, E., Veres, P. R., Wang, S., Allen, H. M., Asher, E., Bian, H., Blake, D., Bourgeois, I., Budney, J., Paul Bui, T., Butler, A., Campuzano-Jost, P., Chang, C., Chin, M., Commane, R., Correa, G., Crounse, J. D., Daube, B., Dibb, J. E., Digangi, J. P., Diskin, G. S., Dollner, M., Elkins, J. W., Fiore, A. M., Flynn, C. M., Guo, H., Hall, S. R., Hannun, R. A., Hills, A., Hintsa, E. J., Hodzic, A., Hornbrook, R. S., Greg Huey, L., Jimenez, J. L., Keeling, R. F., Kim, M. J., Kupc, A., Lacey, F., Lait, L. R., Lamarque, J.-F., Liu, J., Mckain, K., Meinardi, S., Miller, D. O., Montzka, S. A., Moore, F. L., Morgan, E. J., Murphy, D. M., Murray, L. T., Nault, B. A., Andrew Neuman, J., Nguyen, L., Gonzalez, Y., Rollins, A., Rosenlof, K., Sargent, M., Schill, G., Schwarz, J. P., St. Clair, J. M., Steenrod, S. D., Stephens, B. B., Strahan, S. E., Strode, S. A., Sweeney, C., Thames, A. B., Ullmann, K., Wagner, N., Weber, R., Weinzierl, B., Wennberg, P. O., Williamson, C. J., Wolfe, G. M., and Zeng, L.: THE NASA ATMOSPHERIC TOMOGRAPHY (ATom) MISSION: Imaging the Chemistry of the Global Atmosphere, Bull. Am. Meteorol. Soc., 103, E761-E790, https://doi.org/10.1175/BAMS-D-20-0315.1, 2022.

Tiedtke, M.: Representation of clouds in large-scale models, Mon. Weather Rev., 121, 3040–3061, https://doi.org/10.1175/1520-0493(1993)121<3040:ROCILS>2.0.CO;2, 1993.

Wang, H., Easter, R. C., Zhang, R., Ma, P., Singh, B., Zhang, K., Ganguly, D., Rasch, P. J., Burrows, S. M., Ghan, S. J., Lou, S., Qian, Y., Yang, Y., Feng, Y., Flanner, M., Leung, L. R., Liu, X., Shrivastava, M., Sun, J., Tang, Q., Xie, S., and Yoon, J.: Aerosols in the E3SM Version 1: New Developments and Their Impacts on Radiative Forcing, J. Adv. Model. Earth Syst., 12, e2019MS001851, https://doi.org/10.1029/2019MS001851, 2020.

Wang, D., Zhu, B., Wang, H., and Sun, L., Simulation study on the indirect effect of sulfate on the summer climate over the eastern China monsoon region, Sci. Rep., 11, 8295, https://doi.org/10.1038/s41598-021-87832-5, 2021.

Williamson, C. J., Kupc, A., Axisa, D., Bilsback, K. R, Bui, T. P., Campuzano-Jost, P., Dollner, M., Froyd, K. D., Hodshire, A. L., Jimenez, J. L., Kodros, J. K., Luo, G., Murphy, D. M., Nault, B. A., Ray, E. A., Weinzierl, B., Wilson, J. C., Yu, F., Yu, P., Pierce, J. R., and Brock, C. A.: A large source of cloud condensation nuclei from new particle formation in the tropics, Nature, 574, 399–403, https://doi.org/10.1038/s41586-019-1638-9, 2019.

Yan, J., Jung, J., Zhang, M., Xu, S., Lin, Q., Zhao, S., and Chen, L.: Significant Underestimation of Gaseous Methanesulfonic Acid (MSA) over Southern Ocean, Environ. Sci. Technol., 53 (22), pp. 13064-13070, https://doi.org/10.1021/acs.est.9b05362, 2019.

Yu, P. F., Froyd, K. D., Portmann, R.W., Toon, O. B., Freitas, S. R., Bardeen, C. G., Brock, C., Fan, T. Y., Gao, R. S., Katich, J. M., Kupc, A., Liu, S., Maloney, C., Murphy, D. M., Rosenlof, K. H., Schill, G., Schwarz, J. P., and Williamson, C.: Efficient In-Cloud Removal of Aerosols by Deep Convection, Geophys. Res. Lett., 46, 1061–1069, https://doi.org/10.1029/2018gl080544, 2019.

Zhang, K., Zhang, W., Wan, H., Rasch, P. J., Ghan, S. J., Easter, R. C., Shi, X., Wang, Y., Wang, H., Ma, P.-L., Zhang, S., Sun, J., Burrows, S. M., Shrivastava, M., Singh, B., Qian, Y., Liu, X., Golaz, J.-C., Tang, Q., Zheng, X., Xie, S., Lin, W., Feng, Y., Wang, M., Yoon, J.-H., and Leung, L. R.: Effective radiative forcing of anthropogenic aerosols in E3SM version 1: historical changes, causality, decomposition, and parameterization sensitivities, Atmos. Chem. Phys., 22, 9129–9160, https://doi.org/10.5194/acp-22-9129-2022, 2022.

Zhu, J., Penner, J. E., Lin, G., Zhou, C., Xu, L., and Zhuang, B.: Mechanism of SOA formation determines magnitude of radiative effects. Proceedings of the National Academy of Sciences of the United States of America, 114, 12685–12690, https://doi.org/10.1073/pnas.1712273114, 2017.

Zhu, J., Penner, J. E., Yu, F., Sillman, S., Andreae, M. O., and Coe, H.: Decrease in radiative forcing by organic aerosol nucleation, climate, and land use change. Nature Commun, , 10, 423, https://doi.org/10.1038/s41467-019-08407-7, 2019.

Table 1. ATom sulfur measurements used in the study

	SO_4		SO_2		MSA		DMS	
Instrument	AMS[a]	PALMS[b]	CIMS[c]	LIF[d]	AMS	PALMS	TOGA[e]	WAS[f]
ATom deployment(s)	1 to 4	1 to 4	1 to 4	4	1 to 4	1 to 4	2 to 4	1 to 4
Frequency	60 s	180 s	1 s	1 s	1 s	180 s	120 s	Variable but ~180 s
Accuracy	±35% (2s)	±60% at 10 ng m-3 ±20% at 1 µg m-3	±25%	± 9% (1s)	±35% (2s)	±70%	15% or better	15%
precision			130pptv					10%
Detection limit	5-15 ng sm^{-3}	~10 ng sm^{-3}		2 pptv	2.5 ng sm-3 (60 s)	~15 ng sm^{-3}	1 ppt	1 ppt
Cut-off size (dry diameter)	~0.75 µm	0.1-3 µm			~0.75 µm	0.1-3 µm		
Primary Investigator(s)	Jose Jimenez and Pedro Campuzano Jost	Karl Froyd and Gregory Schill	Paul Wennberg	Andrew Rollins	Jose Jimenez and Pedro Campuzano Jost	Karl Froyd and Gregory Schill	Eric Apel	Donald Blake
References	Guo et al., 2021; Schueneman et al., 2021	Froyd et al., 2019	Allen et al., 2022; Crounse et al., 2006	Rollins et al., 2016	Hodshire et al., 2019	Froyd et al., 2019	Apel et al., 2015	Simpson et al., 2001

[a]AMS: Aerosol Mass Spectrometer
[b]PALMS: Particle Analysis by Laser Mass Spectrometry
[c]CIMS: Chemical Ionization Mass Spectrometer
[d]LIF: Laser Induced Fluorescence
[e]TOGA: NCAR Trace Organic Gas Analyzer
[f]WAS: Whole Air Sampler

Table 2. AeroCom Models used in this study

Model Abbreviation	Model Version	Nominal Resolution	Vertical Levels	Meteorological Fields	Ocean Surface Temperature Data	Interactive Aerosol-Meteorology	Endogenous Oxidants	Endogeous DMS Emission	Aerosol Module	Anthropogenic Emission	Volcano Emission	Key References
CAM-ATRAS	CAM5-ATRAS2	1.9° × 2.5°	30	MERRA-2	HadSST	Yes	Yes	No	Microphysics, 12 sectional size bins, and internal mixing of aerosol constituents in each bin.	CEDS (Hoesly et al., 2018),	Degassing (Andres and Kasgnoc, 1998), Eruption (Neely and Schmidt, 2016)	Liu and Matsui 2021; Matsui 2017; Matsui and Mahowald, 2017
E3SM	v1.0	1° × 1°	72	ERA-Interim	HadSST	Yes	No	No	Microphysics, MAM4, internal mixing within a mode, external mixing between modes	CEDS (Hoesly et al., 2018)	Contineous emission (Denener et al., 2006). No eruptive emissions.	Rasch et al., 2019; Wang et al., 2020; Zhang et al. 2022
GEOS	Icarus-3_3_p2	1° × 1°	72	MERRA-2	MERRA_sst	Yes	No	Yes	GOCART, Bulk, external mixing	CEDS (Hoesly et al., 2018)	Carns et al., 2016, 2017	Bian 2017; Colarco et al., 2010; Chin et al., 2000
IMPACT		1.9° × 2.5°	30	Open IFS ECMWF	HadSST	No	Yes	no	Microphysics, internal mixing within a mode, external mixing between modes	CEDS (Hoesly et al., 2018)	AeroCom volcanic emissions	Zhu et al., 2017; Zhu et al., 2019
OsloCTM3	OsloCTM3v1.02	2.25° × 2.25°	60	Open IFS ECMWF	Open IFS ECMWF	No	Yes	Yes	Bulk, external mixing	SSP245 with linear interpolatio n for 2017	AeroCom volcanic emissions, continuous from Dentener (2006)	Lund et al., 018; Søvde et al., 2012

Table 3. DMS emission used/calcuated by the five AeroCom models

Model abbreviation	Emission inventory	DMS concentration in sea water	DMS flux calculation	Meteorological fields
CAM-ATRAS	No	Lana et al. (2011)	Nightingale et al. 2000	Wind from ECMWF-IFS
E3SM	Yes			
GEOS	No	Lana et al. (2011)	Liss and Merlivat, (1986), Saltzman et al. (1993)	SST and wind from GEOS
IMPACT	Yes			
OsloCTM3	No	Kettle and Andreae (2000)	Nightingale et al. (2000)	Wind from ECMWF-IFS

Table 4. Global sulfur budget in 2017

		Emission	$SUPSO_2$[1]	SUPMSA	$SUPSO_4$	Dry	Wet	TotalSource	Burden	Lifetime
		TgS/yr	TgS/yr	TgS/yr	TgS/yr	TgS/yr	TgS/yr	TgS/yr	TgS	days
CAM-ATRAS	DMS	26.05	-26.05	--	--	--	--	26.05	0.13	1.8
	SO2	68.67	26.05	--	-55.67	-39.05		94.72	0.445	1.7
	SO4	1.76	--	--	55.67	-4.72	-53.23	58.09	0.67	4.2
E3SM	DMS	19.43	-19.40	--	--	--	--	19.43	0.0658	1.24
	SO2	67.92	19.40	--	-38.56	-48.76		87.32	0.3825	1.60
	SO4	1.74	--	--	38.56	-6.95	-33.31	40.31	0.6183	5.60
GEOS	DMS	15.57	-14.84	-0.74	--	--	--	15.57	0.0252	0.59
	SO2	67.06	14.84		-37.49	-32.93	-11.39	81.90	0.3488	1.55
	SO4	1.68	--	--	37.49	-5.27	-33.90	39.17	0.3269	3.05
	MSA	--	--	0.74	--	-0.10	-0.64	-.74	0.0063	3.11
IMPACT	DMS	18.22	-18.22	--	--	--	--	18.05	0.0369	0.75
	SO2	64.76	18.22	--	-51.44	-31.29	--	82.98	0.4134	1.82
	SO4	1.36	--	--	51.44	-3.48	-49.32	52.80	0.7502	5.19
OsloCTM3	DMS	26.93	-26.93	--	--	--	--	26.93	0.1496	2.03
	SO2	52.80	26.93	--	-49.23	-29.01	-1.49	79.73	0.2346	1.08
	SO4	1.053	--	--	55.49	-6.35	-50.29	56.54	0.8681	5.60

[1]$SUPSO_2$: chemical production for SO_2

Table 5. Global and annual sulfate multimodel mean and diversity from three AeroCom phases

	AeroCom-I	AeroCom-II		AeroCom-III	
reference	Textor et al., 2006	Myher et al., 2013	Kipling et al., 2016	Gliß et al., 2021	This work
Study year	2000	2006	2006	2010	2017
# of models	16	16	18	14	5
MMM (Tg)	2.0	1.05	1.48	1.87	1.94
δ (%)	25.0	26.4	34.6	38.8	28.0
observation	No	No	No	AC, AS, AE, and AOD from Ground station and AOD from MODIS	DMS, SO_2, SO_4 and MSA from ATom

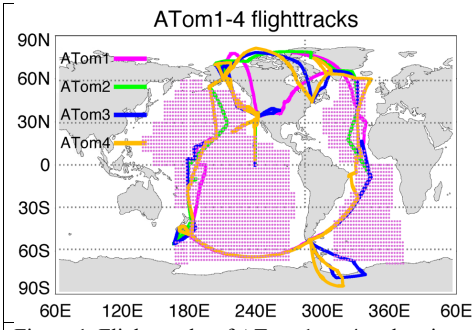

Figure 1. Flight tracks of ATom-1 to -4 and regions for the analysis of SO_4 source origins (shaded area). Periods of the four ATom deployments are ATom-1 (July-August 2016), ATom-2 (January-February 2017), ATom-3 (September-October 2017) and ATom-4 (April-May 2018).

1334

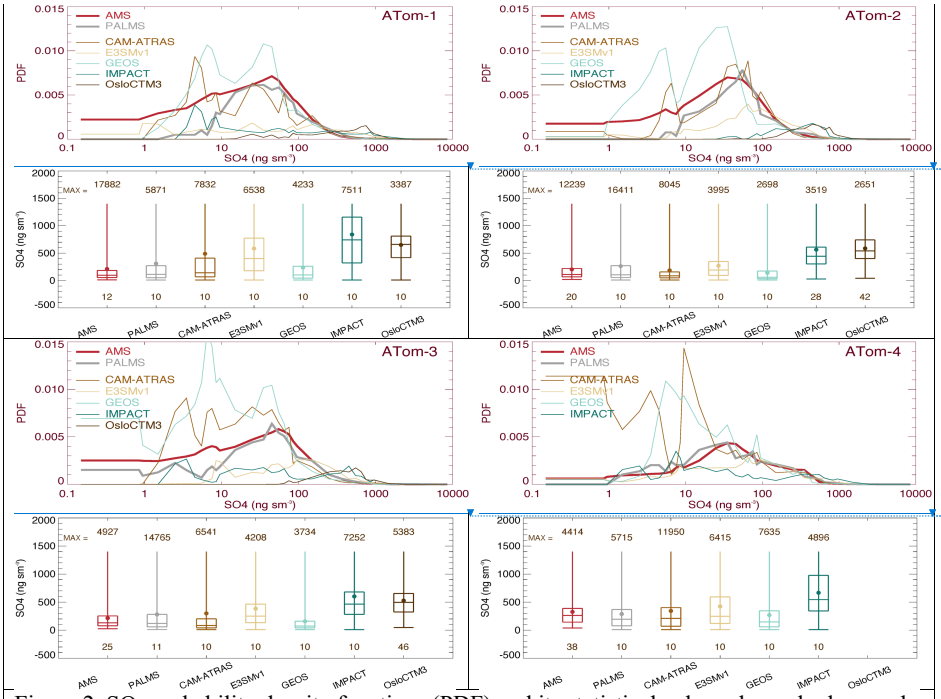

Figure 2. SO_4 probability density functions (PDF) and its statistical values shown by box-and-whisker for the four ATom deployments. All data (AMS in red, PALMS in grey, and five model simulations in other colors) are sampled at 10-s points. Statistical values include the range of the data from minimum to maximum, the three levels of the 25th, 50th (median), and 75th percentiles in the box, and the filled circle for the mean. Statistical values are calculated when measured values are above the detection limit (DL).

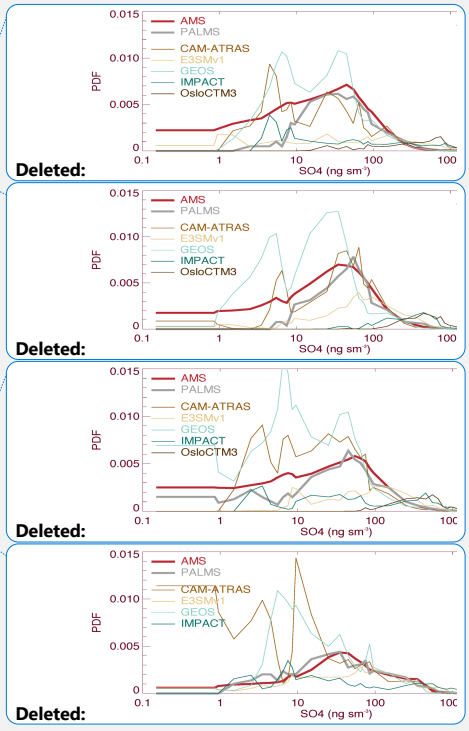

Deleted: Statistical values include the range of the data from minimum to maximum, the three levels of the 25th, 50th (median), and 75th percentiles in the box, and the filled circle for the mean.

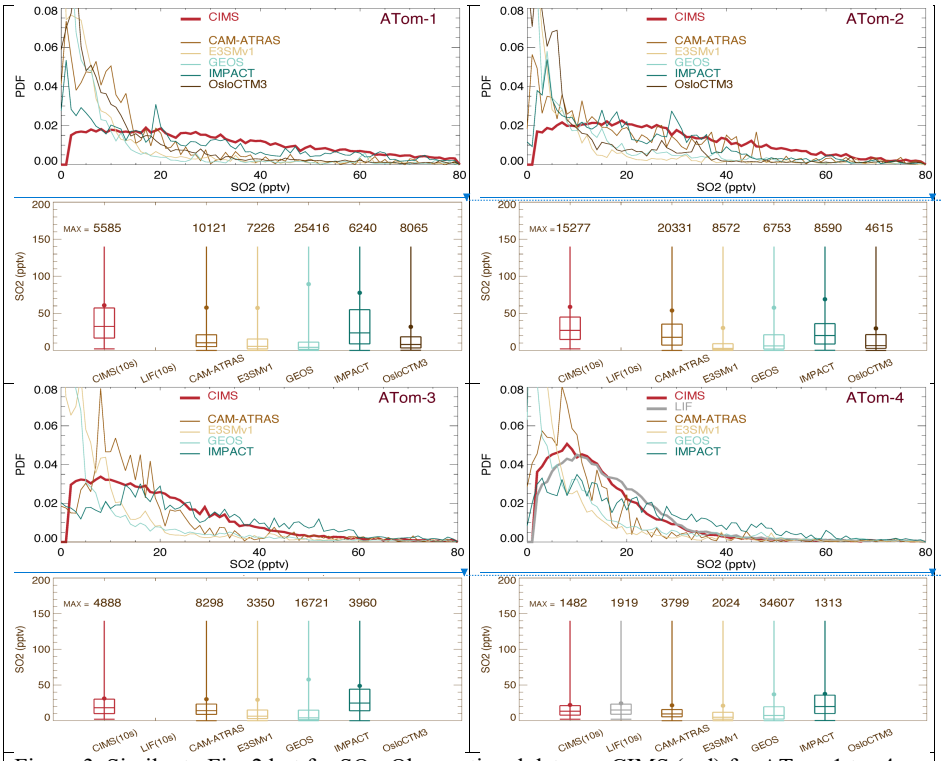

Figure 3. Similar to Fig. 2 but for SO_2. Observational data are CIMS (red) for ATom-1 to -4 and LIF (grey) for ATom-4 from ATom 10-s merged data. PDFs and statistical values are calculated at points where CIMS (and LIF in ATom-4) measured SO_2 are above DL (e.g., 2 pptv).

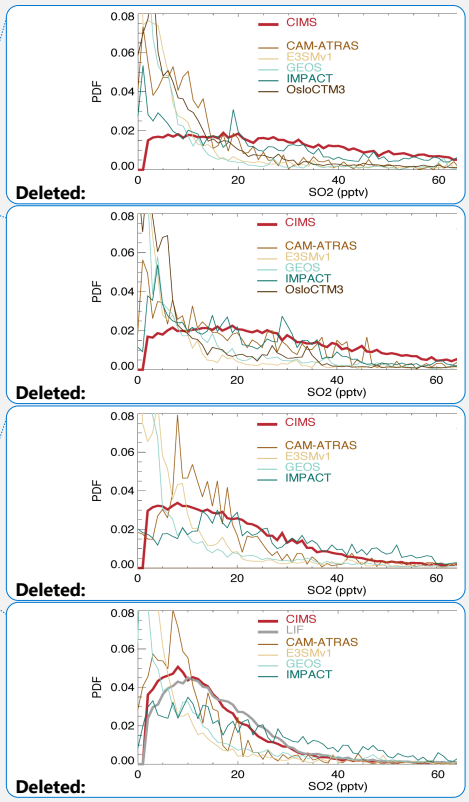

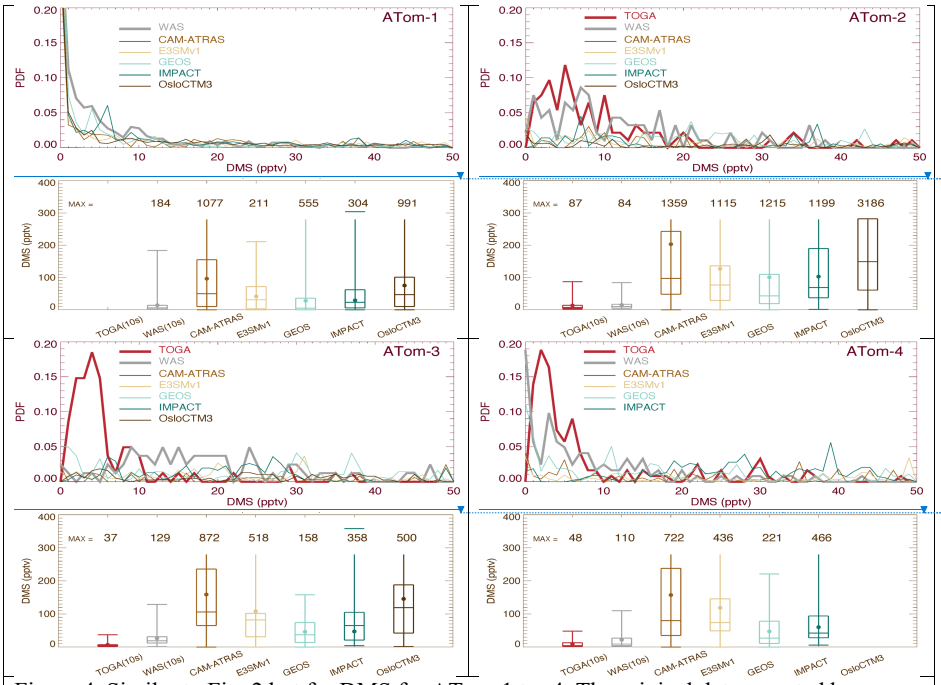

Figure 4. Similar to Fig. 2 but for DMS for ATom-1 to -4. The original data reported by TOGA (e.g., 35-s) and by WAS (e.g., ~60-s) have also been converted to 10-s frequency. Data included in PDF and statistical analysis are on 10-s points where DMS measured by both TOGA and WAS are above DL (i.e., 1 pptv).

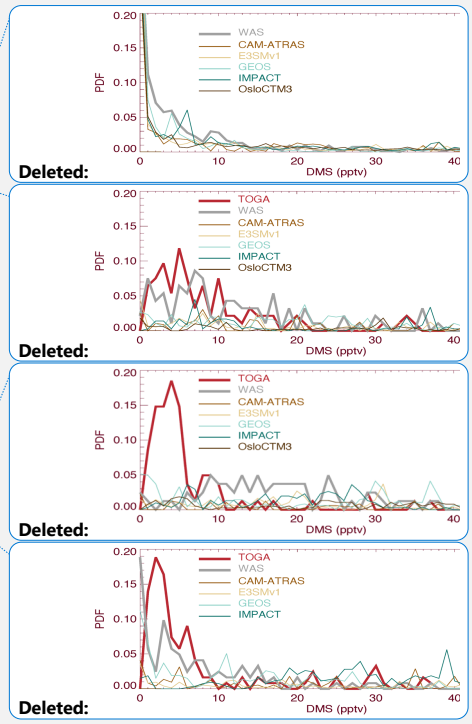

1361

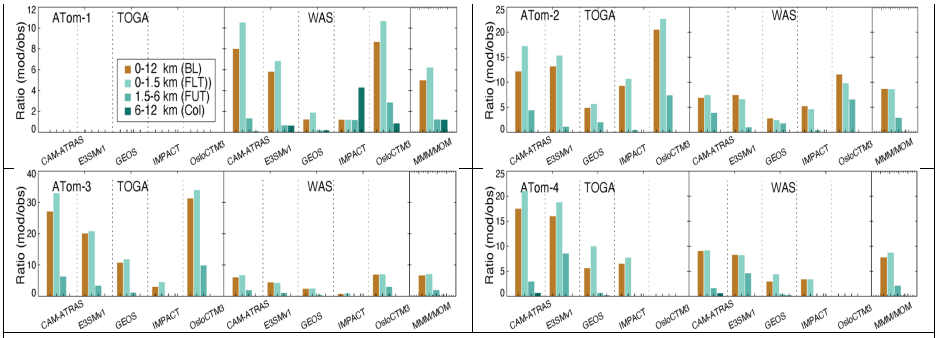

Figure 5. Ratio of DMS median values between model simulation and observation for four ATom deployments. Ratio analyses are performed on four vertical ranges as shown in four colors (see legend in ATom-1). The last column "MMM/MOM" refers to multi-model median to multi-observation median.

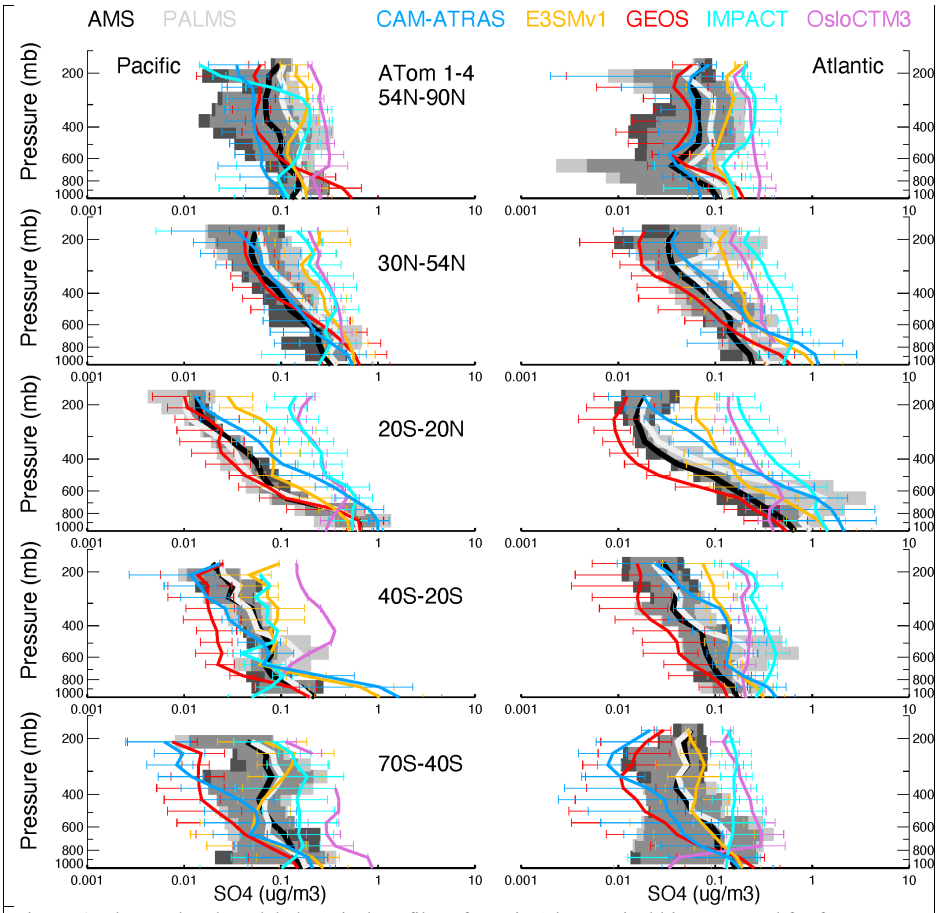

Figure 6. Observed and modeled vertical profiles of SO_4 in 1-km vertical bins averaged for four ATom deployments (lines) and variation across the four ATooms (shaded area for measurements and horizontal bars for simulations). ATom measurements are shown in black (AMS) and light grey (PALMS) while model results are shown in other colors. Comparisons are conducted only when both observational measurements above detect limitation are available. Comparisons are separated into five latitude bands from the Northern to the Southern Hemisphere, and into Pacific and Atlantic Basins.

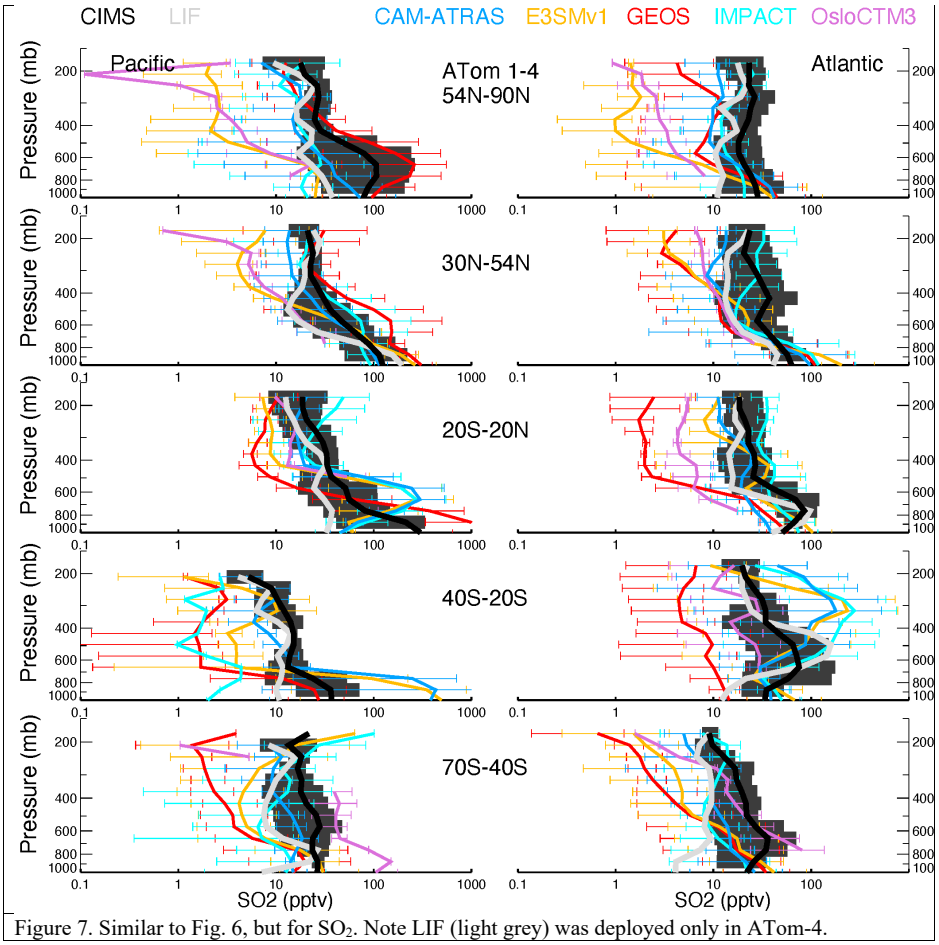

Figure 7. Similar to Fig. 6, but for SO_2. Note LIF (light grey) was deployed only in ATom-4.

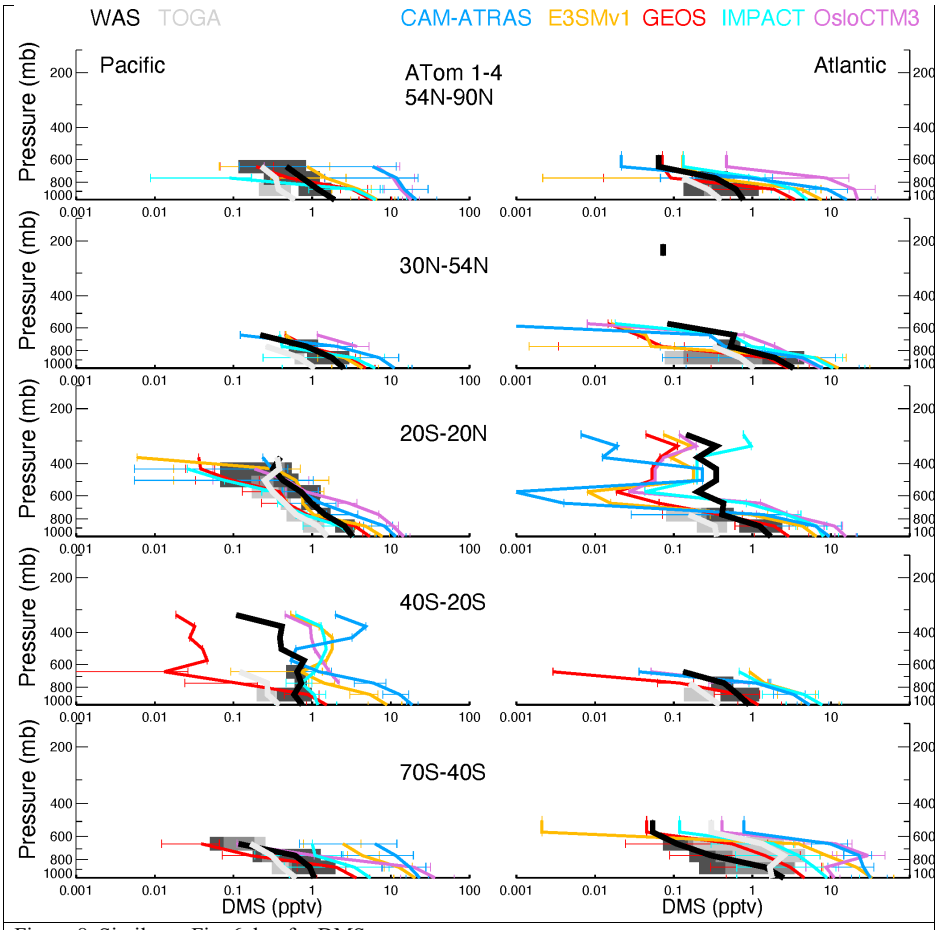

Figure 8. Similar to Fig. 6, but for DMS.

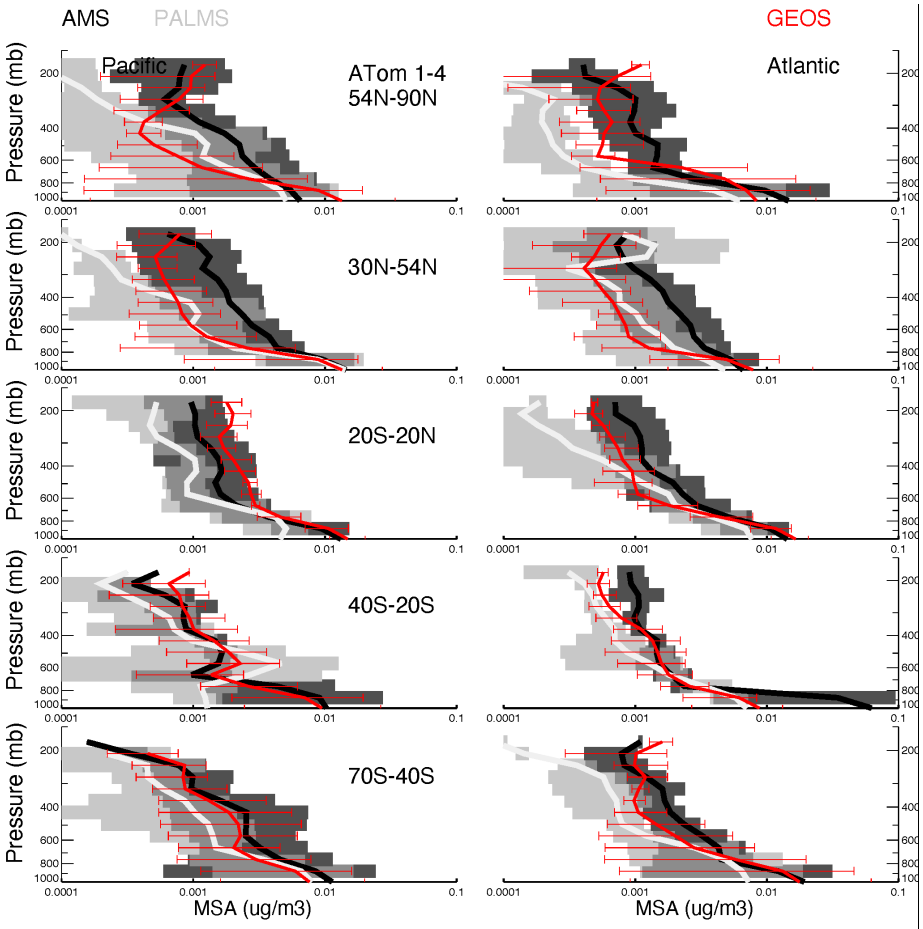

Figure 9. Similar to Fig. 6, but for MSA.

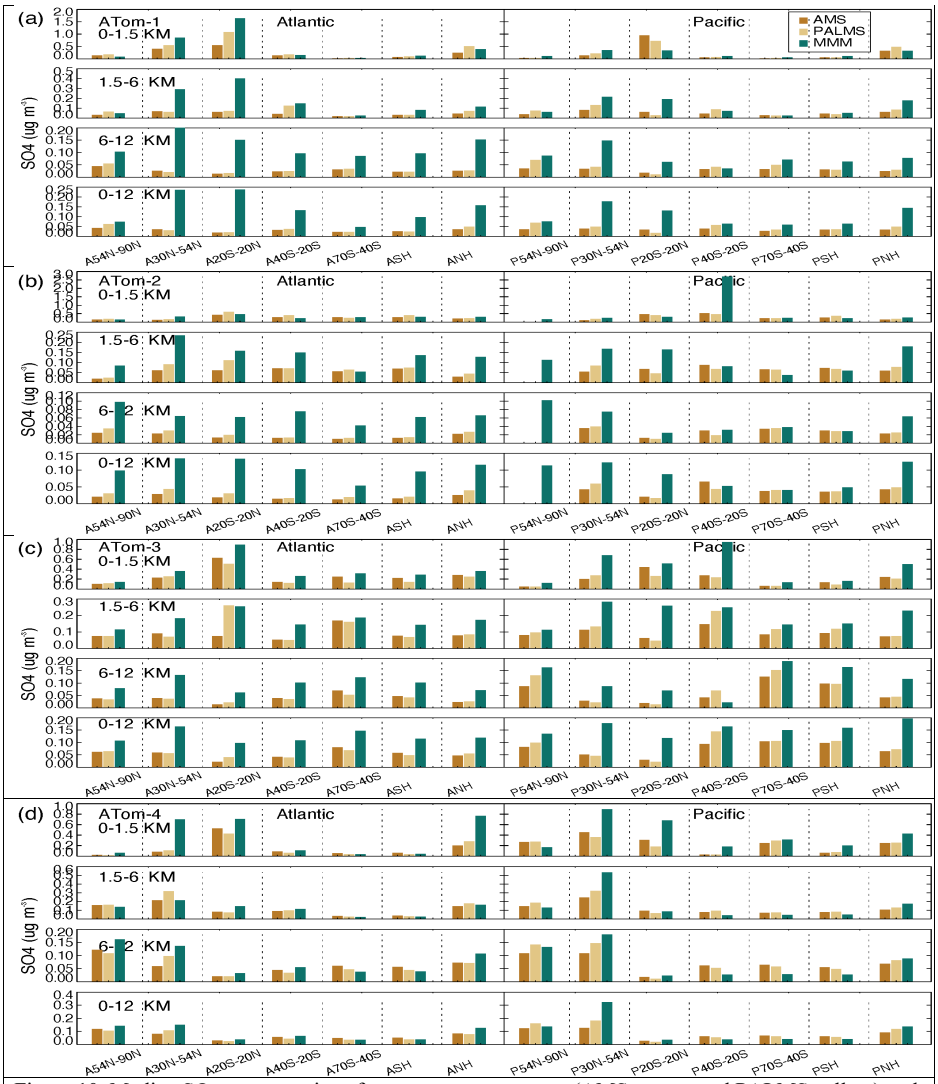

Figure 10. Median SO_4 concentrations from two measurements (AMS orange and PALMS yellow) and multi-model simulation (green) at seven latitudinal bands (including SH and NH) and four vertical layers (i.e., 0-1.5 km, 1.5-6 km, 6-12km, and 0-12 km) over Atlantic and Pacific oceans for four ATom deployments (a-d).

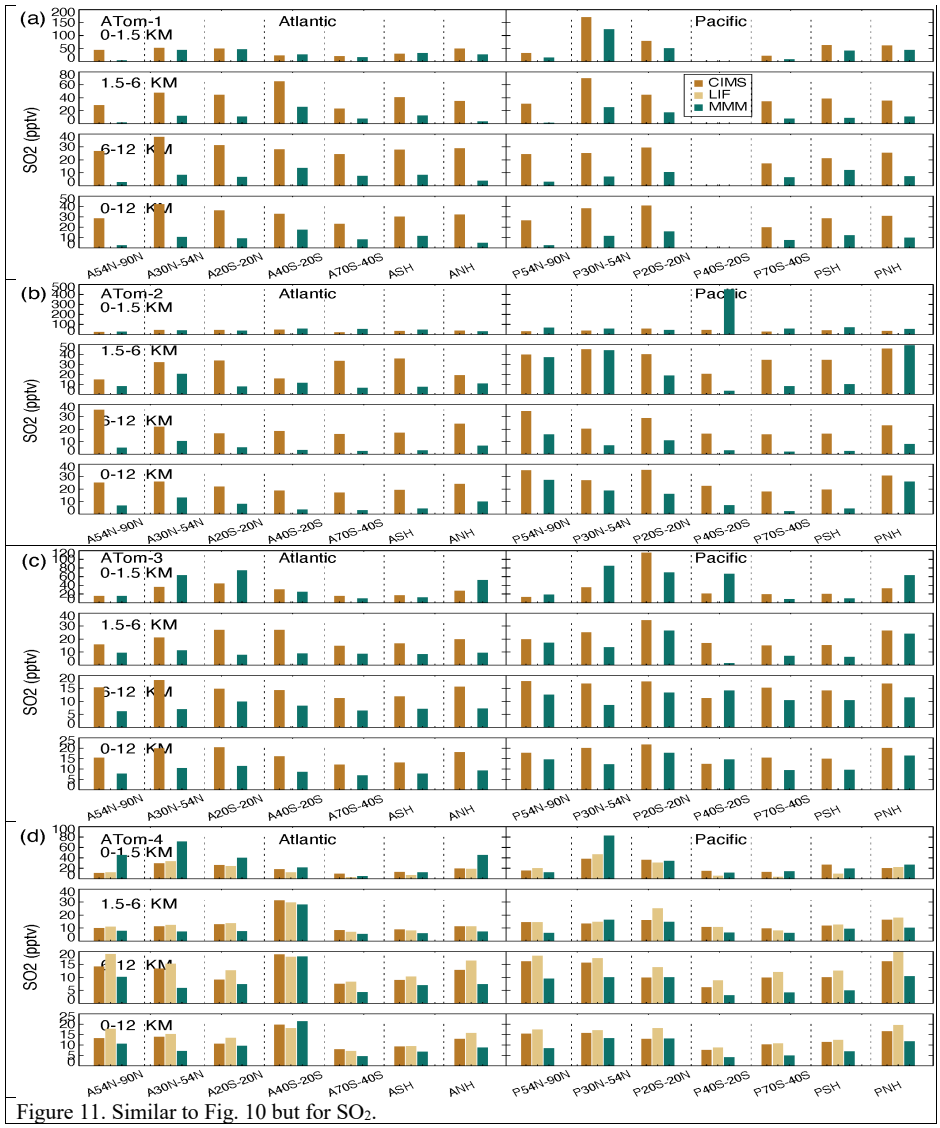

Figure 11. Similar to Fig. 10 but for SO_2.

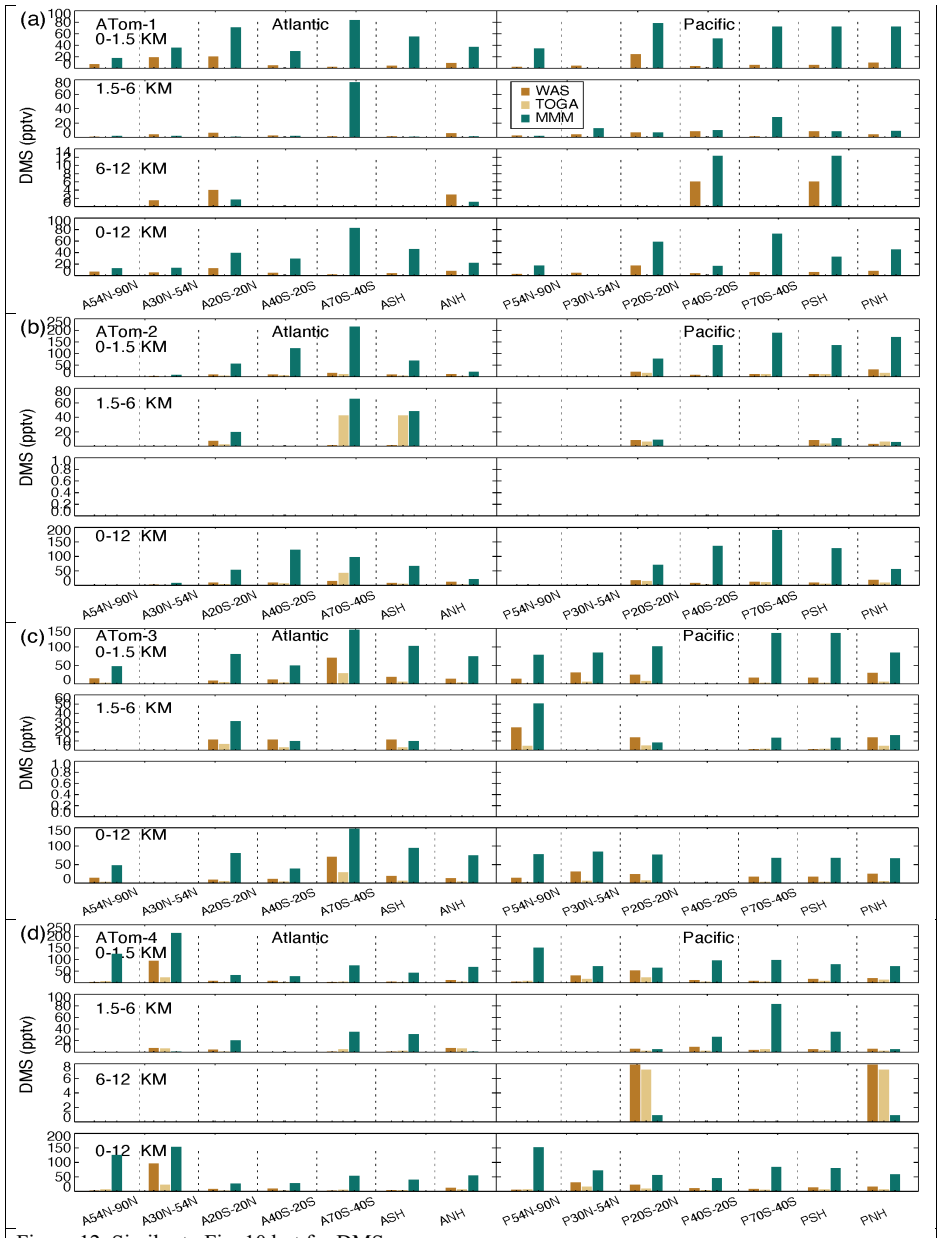

Figure 12. Similar to Fig. 10 but for DMS.

1402

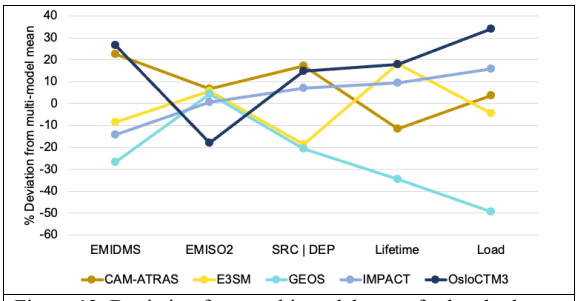

Figure 13. Deviation from multi-model mean for key budget items in sulfur study include DMS emission, SO_2 emission, sulfate source or total deposition, sulfate lifetime, and total sulfate atmospheric mass load.

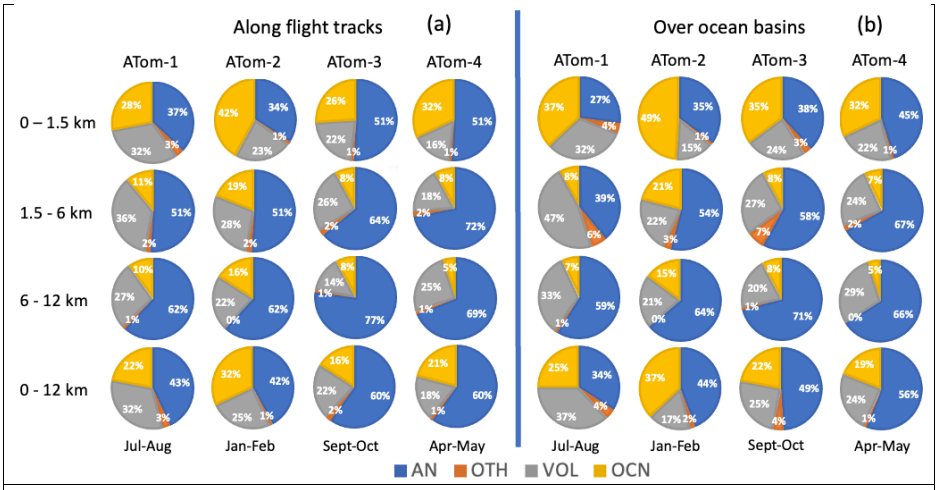

Figure 14. Source origins in percentage (%) for aerosol SO_4 along flight tracks (a) and for a wide oceanic area (b) based on the results from GEOS. Source origins are identified as anthropogenic (AN), volcanic (VOL), oceanic (OCN), and other sources (OTH). Ocean basins include shaded region shown in Fig. 1.

Page 1: [1] Deleted **Bian, Huisheng (GSFC-614.0)[UNIVERSITY OF MARYLAND BALTIMORE CO]**
12/19/23 11:24:00 AM

Page 1: [2] Deleted **Bian, Huisheng (GSFC-614.0)[UNIVERSITY OF MARYLAND BALTIMORE CO]**
12/19/23 11:27:00 AM

Page 1: [3] Deleted **Bian, Huisheng (GSFC-614.0)[UNIVERSITY OF MARYLAND BALTIMORE CO]**
12/19/23 11:28:00 AM